OPEN ACCESS Freely available online

PLoS one

Wingless Directly Represses DPP Morphogen Expression via an Armadillo/TCF/Brinker Complex

Heidi Theisen[1,4☯], Adeela Syed[1,4☯], Baochi T. Nguyen[2], Tamas Lukacsovich[1,4], Judith Purcell[1,4], Gyan Prakash Srivastava[4¤a], David Iron[2¤b], Karin Gaudenz[1,4¤c], Qing Nie[2], Frederic Y. M. Wan[2], Marian L. Waterman[3], J. Lawrence Marsh[1,4]*

1 Department of Developmental and Cell Biology, University of California Irvine, Irvine, California, United States of America, **2** Department of Mathematics, University of California Irvine, Irvine, California, United States of America, **3** Department of Microbiology and Molecular Genetics, University of California Irvine, Irvine, California, United States of America, **4** Developmental Biology Center, University of California Irvine, Irvine, California, United States of America

Background. **Spatially restricted morphogen expression drives many patterning and regeneration processes, but how is the pattern of morphogen expression established and maintained? Patterning of *Drosophila* leg imaginal discs requires expression of the DPP morphogen dorsally and the wingless (WG) morphogen ventrally. We have shown that these mutually exclusive patterns of expression are controlled by a self-organizing system of feedback loops that involve WG and DPP, but whether the feedback is direct or indirect is not known.** ***Methods/Findings.*** **By analyzing expression patterns of regulatory DNA driving reporter genes in different genetic backgrounds, we identify a key component of this system by showing that WG directly represses transcription of the *dpp* gene in the ventral leg disc. Repression of *dpp* requires a tri-partite complex of the WG mediators armadillo (ARM) and dTCF, and the co-repressor Brinker, (BRK), wherein ARM•dTCF and BRK bind to independent sites within the *dpp* locus.** ***Conclusions/Significance.*** **Many examples of dTCF repression in the absence of WNT signaling have been described, but few examples of signal-driven repression requiring both ARM and dTCF binding have been reported. Thus, our findings represent a new mode of WG mediated repression and demonstrate that direct regulation between morphogen signaling pathways can contribute to a robust self-organizing system capable of dynamically maintaining territories of morphogen expression.**

Citation: Theisen H, Syed A, Nguyen BT, Lukacsovich T, Purcell J, et al (2007) Wingless Directly Represses DPP Morphogen Expression via an Armadillo/TCF/Brinker Complex. PLoS ONE 2(1): e142. doi:10.1371/journal.pone.0000142

INTRODUCTION

Numerous studies have demonstrated that WNT signaling (WG in Drosophila) mobilizes a nuclear β-catenin/TCF complex that can activate transcription of WNT target genes [1–4]. WNT signaling typically leads to the stabilization and nuclear accumulation of ß-catenin ARM (Armadillo), which forms an activating complex with the DNA binding WNT effector TCF (Pangolin or dTCF in Drosophila) [5]. However WNT signaling can also repress gene expression, even within the same cell where WNT activation occurs. In most cases it is unclear if repression is direct or indirect and the molecular mechanisms involved are unknown.

Development of the Drosophila leg imaginal disc requires maintaining complementary territories of dorsal *dpp* and ventral *wg* morphogen expression. We and others have noted that WNT/WG signaling activates *wg* expression and represses *dpp* expression in the ventral territory of the Drosophila leg imaginal disc, and this is critical for normal patterning of the disc [6–11], but whether WNT/WG directs ARM•dTCF complexes to activate expression of repressor proteins or whether ARM•dTCF complexes bind directly to the *dpp* gene to repress transcription is unclear. Here we investigate the mechanism of WG mediated repression of *dpp* and the basis of the self-organizing behavior of the *wg* and *dpp* expression territories (Theisen et al., 1996).

Studies with cultured cells using the WNT activated TOP-FLASH promoter have identified many components that contribute to WNT mediated gene activation. However, the response to WG signaling *in vivo* is often repression of gene expression *e.g.* the *dpp*, *dfrizzled2* (*dfz2*), *stripe* (*sr*), *engrailed* (*en*), *ovo/shavenbaby* (*svb*), and Ubx genes are all repressed upon WG signaling [12–18]. It is not known if repression is direct or indirect and little is known about the co-effectors that produce an inhibitory signal versus an activating signal in response to WG signaling. To determine whether repression by WG signaling is direct or indirect and to better understand the factors that allow a WG signal to be inhibitory, we investigated whether dTCF binds to the *dpp* gene and whether dTCF and/or ARM are required for WG directed repression.

Here, we show that a novel WG dependent repressing complex that includes ARM•dTCF and the co-repressor Brinker binds

Academic Editor: Carl-Philipp Heisenberg, Max Planck Institute of Molecular Cell Biology and Genetics, Germany

Received September 29, 2006; **Accepted** December 8, 2006; **Published** January 3, 2007

Funding: This work was supported by NIH grants RO1 HD36081 and RO1 HD36049 to JLM and NIH CA83982 to MLW, by NIH GM067247 and GM75309 to QN and FW through the Joint NSF/NIGMS Initiative to Support Research in the Area of Mathematical Biology, by NSF SCREMS Grant #DMS0112416, P20GM066051 JLM, QN, FW and by the Chao Family Comprehensive Cancer Center Functional Genomics Program. HT was supported in part by a PHS training grant 5T32 GM07311-17. This work was made possible, in part, through access to the confocal facility and Biacore facility of the Optical Biology Shared Resource of the Cancer Center Support Grant (CA-62203) at the University of California, Irvine.

Competing Interests: The authors have declared that no competing interests exist.

* **To whom correspondence should be addressed.** E-mail: jlmarsh@uci.edu

☯ These authors contributed equally to this work.

¤a **Current address:** Computer Science Department, University of Missouri-Columbia, Columbia, Missouri, United States of America
¤b **Current address:** Department of Mathematics and Statistics, Dalhousie University, Halifax, Nova Scotia, Canada
¤c **Current address:** Stowers Institute, Kansas City, Missouri, United States of America

directly to the *dpp* enhancer region to provide a key component of a self organizing regulatory loop.

RESULTS

Identifying a WG response element in the *dpp* regulatory domain

The *wg* and *dpp* genes are expressed in non-overlapping ventral and dorsal domains respectively in the leg imaginal disc of Drosophila. Loss of WG signaling leads to ectopic transcription of *dpp* and an engineered gain of WG signaling can suppress *dpp* transcription [6–11]. To determine if repression of *dpp* by WG is direct or indirect, we identified WG-responsive sequences within the *dpp* gene. The *dpp* gene is regulated by an extensive set of enhancers some of which are located approximately 30 kb downstream of the *dpp* coding region (Fig. 1A; [19]). A 10 kb fragment from this region (BS3.0; 106.9–116.9; Fig. 1A; [19]) directs β-galactosidase expression in the normal pattern of *dpp* expression in imaginal discs (Fig. 1B,C). In the leg disc, expression occurs in a stripe along the anterior/posterior (A/P) compartment boundary, except that extension of the stripe into the ventral region is prevented by WG-dependent repression (Fig. 1B,C) [6–11,20,21]. Since WG signaling is mediated via ARM•dTCF complexes, we scanned the 10 kb *dpp* enhancer fragment and found 8 potential dTCF binding sites [22], 5 of which fell into two clusters within 2kb of each other in a region that is able to direct expression in leg imaginal discs (Fig. 1A; APRD). A proximal cluster (P) is located around map coordinates 110 and is contained within fragments that activate *dpp* along the entire A/P boundary. Based on the location of these sites, we analyzed a series of *dpp* enhancer fragments in transgenic flies (Fig. 1A). At least 4 independent transformant lines were examined for each construct; and the expression patterns were the same for each line tested.

The smallest reporter construct that contains all the elements necessary to mimic the normal *dpp* expression pattern is a 2.8 kb *dpp* enhancer fragment that includes an activating region (A), the proximal dTCF cluster (P), a co-repressor binding region (R), and a distal cluster of dTCFsites (D) (APRD; 109.5–112.3) (Fig. 1D). We designate these four functional regions of the 2.8 kb enhancer as APRD with dashes to denote deletion of particular regions and lower case italics to denote regions in which specific dTCF binding sites have been mutated.

An 800 bp fragment containing both the activating region (A), and the proximal cluster of dTCF sites (P) [(BS3.1, AP--) [19]; 109.5–110.3] activates transcription along the A/P boundary but does not exhibit ventral repression (Fig. 1F). The downstream 2 kb region (--RD), containing the putative co-repressor binding element (R), and the distal cluster of dTCF sites (D), is required for repression but cannot itself activate expression [BS3.2 [19]; 110.3–112.3; Fig. 1A; data not shown]. Deleting the 1.4 kb R region of DNA between the dTCF clusters (AP-D)(Fig. 1A;G) or removing a 500 bp fragment that contains the distal cluster of dTCF sites (APR-)(Fig. 1A;E), results in loss of ventral repression. These data show that repression requires at least two regions in the adjacent 2 kb, namely the distal cluster of dTCF sites (D) and a co-repressing region (R) that does not contain dTCF sites. Genomic fragments that lack the 800 nucleotide AP fragment (Fig. 1A, --RD, BS3.2 of Blackman) are not expressed at all and hence repression cannot be evaluated [*e.g.* Blk2.5; 106.9–109.3, and BS3.2, [19] Fig. 1A; data not shown]. Thus, the minimal region necessary for proper *dpp* regulation in the leg disc is the 2.8 kb APRD fragment that contains distinct activating (A) and repressing sequences (RD).

The 2.8 kb *dpp* enhancer, APRD, responds to WG signaling

To determine if the *dpp* reporter constructs are responsive to WG signaling, we examined reporter gene expression in animals where WG signaling is blocked at the level of the ligand and at the level of ARM/dTCF. A temperature sensitive *wg* allele, wg^{IL114} [23], was used to test the effect of WG signaling on the expression of both the 10 kb (BS3.0) and the 2.8 kb *dpp* enhancer (APRD) fragments (Fig. 2A,B). Repression of both the 10 kb and 2.8 kb (APRD) *dpp* reporters is lost in the ventral region of wg^{ts} discs within 24 h of a temperature shift, indicating that the APRD region of the *dpp* enhancer is responsive to WG directed repression (Fig. 2A,B and data not shown).

To block the nuclear response to WG signaling, we expressed dominant negative dTCF (DNdTCF), which lacks the ARM binding domain [22], and therefore acts as a nuclear repressor of the WG pathway. If repression of *dpp* by WG requires an ARM•dTCF complex, then over-expression of DNdTCF should block repression of *dpp* transcription and result in *dpp* expression in the ventral region. Expression of UAS>DNdTCF was driven with the HS>Gal4 driver and expression of the BS3.0 and APRD enhancer fragments was monitored. Within 2.5 hrs of activating DNdTCF by shifting to 25°C, expression of the *dpp* reporter increased dramatically in the ventral region (compare Fig. 2D vs C). The cell cycle time at this stage was ~6–10 hrs [24,25], therefore, the change in gene expression occurred over the course of ≤1 cell division, suggesting that the regulation of *dpp* gene expression by ARM•dTCF is not an indirect consequence of a regenerative response. To confirm that the endogenous *dpp* gene also responds to DNdTCF, *dpp* expression was monitored in animals where the dpp^{blink}>Gal4 driver was used to drive DNdTCF expression in a pattern that overlaps both the dorsal region of *dpp* expression and the ventral region of *wg* expression in leg discs [26]. Repression of endogenous *dpp* is lost in these discs (not shown). Thus, blocking WG signaling either at the level of ligand activity or at the level of ARM•dTCF complex formation, leads to a rapid loss of *dpp* repression in ventral cells of the leg discs, indicating that repression of *dpp* transcription requires the formation of ARM•dTCF complexes.

Repression of the *dpp* enhancer requires dTCF binding

To evaluate whether the rapid de-repression in response to DNdTCF reflects competition for dTCF binding sites within the *dpp* locus or an indirect effect being mediated through other factors, we sought to map and mutate the putative dTCF binding sites in the *dpp* regulatory region. DNAse I footprinting analysis with both recombinant dTCF protein and with human LEF-1 protein showed that both the Drosophila and human proteins protect all 5 putative TCF binding sites in the APRD *dpp* fragment (Fig. 3A, B and data not shown). We also performed electrophoretic mobility shift assays to confirm that these sites were the only *bona fide* dTCF binding sites and that there were no other dTCF binding sites within the APRD region (data not shown).

To test whether direct binding of dTCF to the 2.8 kb *dpp* enhancer fragment is required for *dpp* regulation, we engineered specific inactivating mutations in all 5 dTCF binding sites (A*p*R*d*) or only in the distal cluster of 3 dTCF sites (APR*d*). Gel shift experiments with recombinant dTCF demonstrated that the introduced mutations eliminated dTCF binding (data not shown). We compared the expression of the *dpp* reporter gene with the dTCF sites intact *vs.* mutated. Loss of binding sites either in both clusters or in only the distal cluster (A*p*R*d* or APR*d*), caused

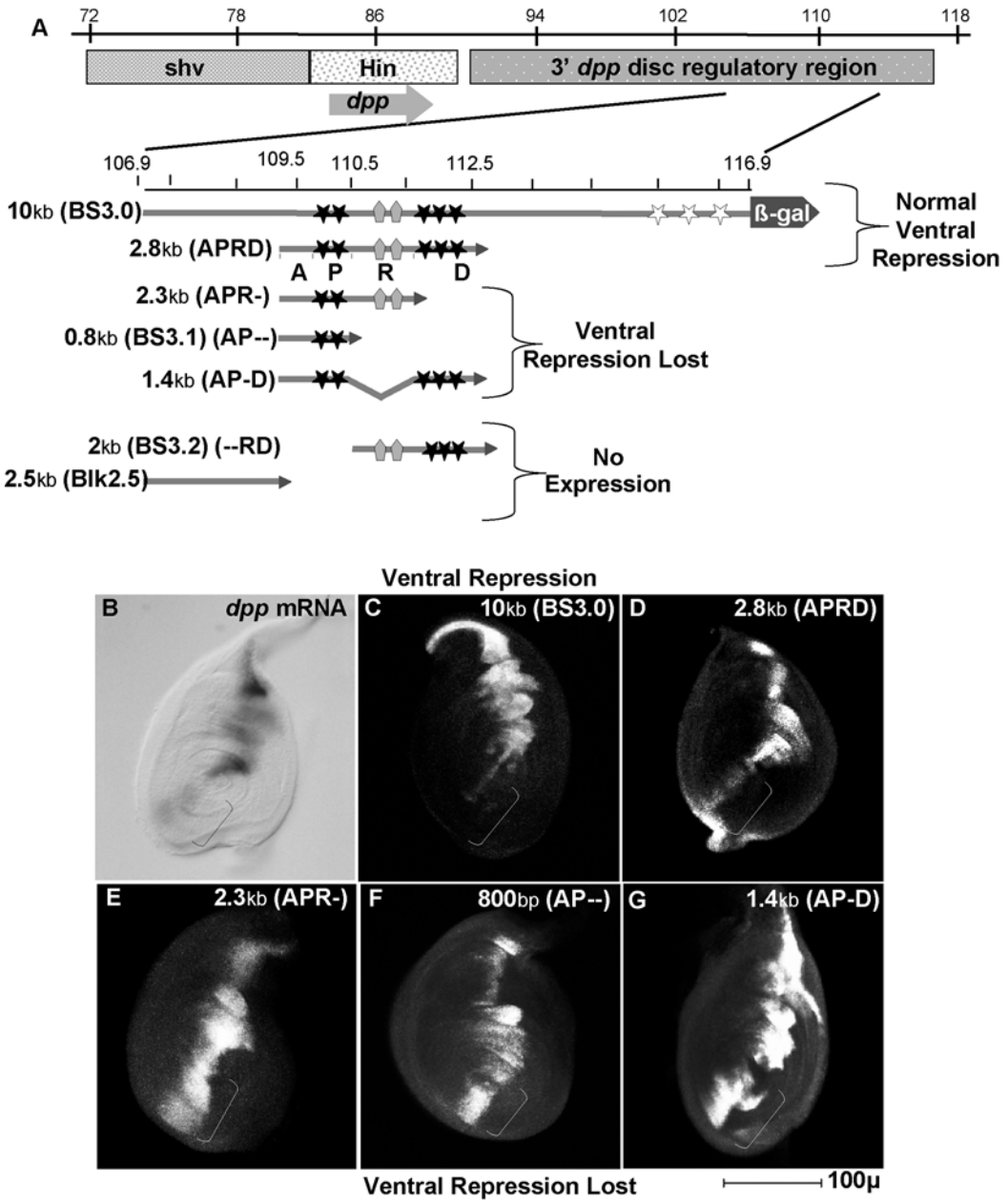

Figure 1. A 2.8 kb fragment of the *dpp* enhancer is sufficient for activation and repression of *dpp* in the leg disc.
A: Schematic representation of the *dpp* locus and the 6 enhancer fragments used in this study. The *dpp* transcription unit is centered around 86 kb (arrow). [Map coordinates (in kilobases) from [19,52,53]. The leg disc enhancer is located between 20–30 kb downstream of the *dpp* coding region. Filled stars represent dTCF-binding sites confirmed by footprinting, open stars are predicted sites and pentagons are BRK binding sites. Arrowheads indicate fusion to the ß galactosidase reporter gene. APRD refers to the 4 relevant domains A (region required for Activation), P (proximal TCF sites), R (repressor domain), D (distal TCF sites). B–E: 3rd instar leg imaginal discs with dorsal up and anterior to the left. B: Normal *dpp* mRNA expression detected by *in situ* hybridization. Bracket indicates ventral region, where *dpp* is repressed. C: A 10 kb *dpp* enhancer fragment (BS3.0) drives expression of lacZ in a stripe that recapitulates normal *dpp* expression including ventral repression (bracket). D: Expression driven by the 2.8 kb APRD *dpp* enhancer fragment mimics *dpp* mRNA and BS3.0 expression. Again, note ventral repression (bracket). E: Ventral repression is lost (bracket) in the 2.3 kb APR- fragment which has a 500 bp region of APRD that contains the distal cluster of dTCF binding sites (D) deleted. F: An 800 bp fragment (AP--, BS3.1) containing the proximal cluster of dTCF sites (P) is not sufficient for ventral repression (bracket). G: The AP-D fragment does not show ventral repression (bracket). Sequences in the 1.4 kb between the proximal and distal dTCF sites do not contain dTCF sites but are required for ventral repression.
doi:10.1371/journal.pone.0000142.g001

a dramatic loss of repression in the ventral leg disc (Fig. 3C–E). As described earlier, the two dTCF sites in the Proximal Cluster of the APRD fragment are not sufficient to cause measurable repression when the distal complex is absent nor are TCF sites required for activation since fragments with all TCF sites mutated still drive expression (not shown). These data demonstrate that binding of dTCF to the distal sites is necessary to inhibit *dpp* transcription. This is further confirmed by finding that mutation of

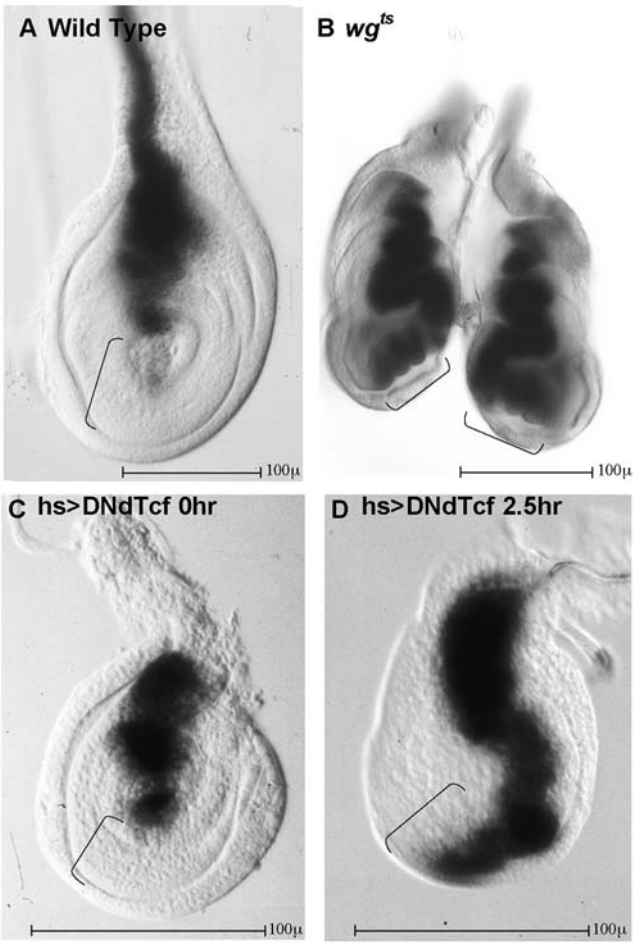

Figure 2. The *dpp* enhancer responds to WG signaling
A–D: 3rd instar leg imaginal discs. Dorsal is up, anterior is to the left. Expression of the 2.8 kb APRD reporter fragment is monitored by β-galactosidase activity. A: In wild type leg discs (mesothoracic shown), APRD>LacZ expression is repressed in the ventral region (bracket). B: WG signaling is required for ventral repression. In a pair of everting prothoracic leg discs from a *wg*^{ts} larva, ventral repression of APRD>LacZ is lost after shifting to restrictive temperature (brackets). C: Expression of the APRD reporter is repressed ventrally in Hs>Gal4; UAS>DNdTCF animals reared at 18° (bracket). DNdTCF is a dominant negative form of dTCF that cannot bind ARM. These animals and their discs are small compared to their non DNdTCF bearing sibs even when maintained continuously at low temperature, presumably due to low level expression of Hs>Gal4. However, these control animals maintained at low temperature do survive as viable, mophologically intact adults. D: When heat shocked in late third instar, repression is lost within 2.5 hours (bracket). At least 6 animals of each genotype were examined and all legs exhibited the same responses.
doi:10.1371/journal.pone.0000142.g002

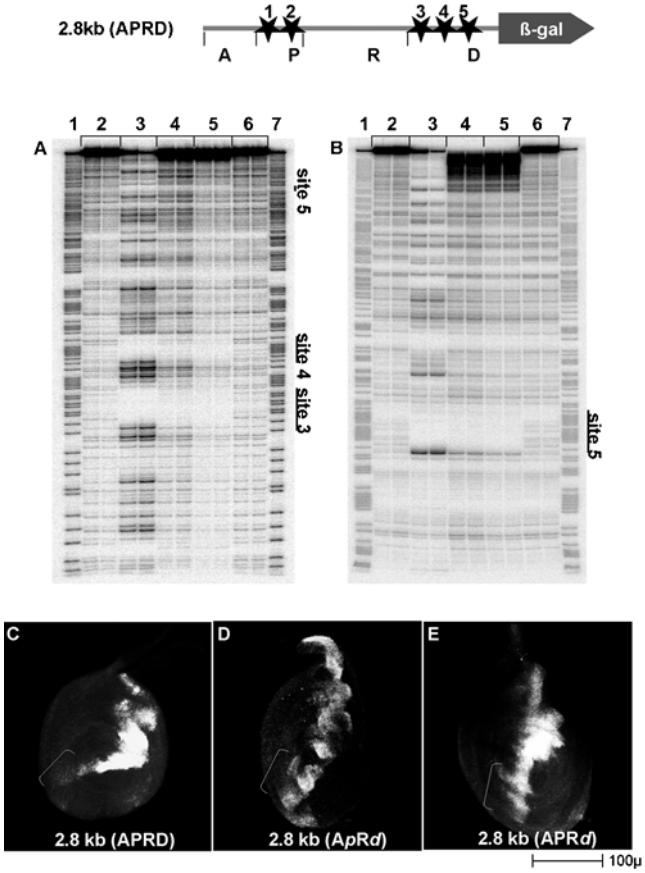

Figure 3. Identification of dTCF binding sites required for *dpp* ventral repression
A,B: dTCF binding sites in the *dpp* regulatory region from 109.4–112.8 kb were mapped by DNase I footprinting using dTCF protein as described in the methods section [22]. The approximate positions of the protected sites are indicated by stars. DNase I footprinting of the region containing the distal cluster (D) reveals 3 protected sites (sites 3, 4; 5) indicated by the bars in A and B. Similar footprints identified two sites in the proximal cluster (sites 1; 2 = P) and no footprints or gel shifts were detected in the A or R regions (not shown). Duplicate lanes represent independent reactions. Lanes 1; 7 are the GA sequencing ladder. All lanes utilize a 1:1 dilution of bacterial extract containing empty expression vector or protein expressing vector and the same concentration of DNaseI except lane 4. Lanes 2 and 6 are no protein controls. Lane 3 uses an extract expressing human LEF1 protein. Lanes 4 and 5 use an extract expressing dTCF with lane 4 containing a 3 times higher concentration of DNase. C–E: 3rd instar leg imaginal discs. Dorsal is up, anterior is to the left. *dpp* lacZ expression is monitored by immunofluorescence. C: The 2.8 kb APRD *dpp* enhancer fragment with all 5 dTCF sites intact is repressed ventrally (bracket). D: Mutation of all 5 dTCF sites (A*p*R*d*) eliminates ventral repression (bracket). E: Mutation of just the 3 distal dTCF sites (APR*d*) is sufficient to eliminate ventral repression (bracket).
doi:10.1371/journal.pone.0000142.g003

the dTCF sites leads to ventral expression that is unresponsive to WG, ARM and dTCF overexpression (Fig. 4A, B and data not shown). Thus, functional dTCF binding sites in the APRD *dpp* enhancer fragment are required for WG dependent repression of *dpp* transcription *in vivo*.

Brinker is required for WG dependent repression of *dpp*

How is it that dTCF binding in response to WG signaling inhibits expression of *dpp* but activates other genes? The AP-D construct, which contains 5 intact dTCF sites but has an internal deletion (Fig. 1G), has lost repression in the ventral region of the leg disc. This suggests that the deleted region contains an element that cooperates with dTCF to repress *dpp* transcription. A scan of this co-repressor region (R) for potential binding sites of known repressors of *dpp* identified two potential Brinker (BRK) sites. BRK is a sequence-specific transcription factor that is repressed by DPP signaling. Furthermore, the expression pattern of *brk* compliments that of *dpp* in the leg disk; there is lower expression along the A/P boundary in the dorsal region, but strong expression in the

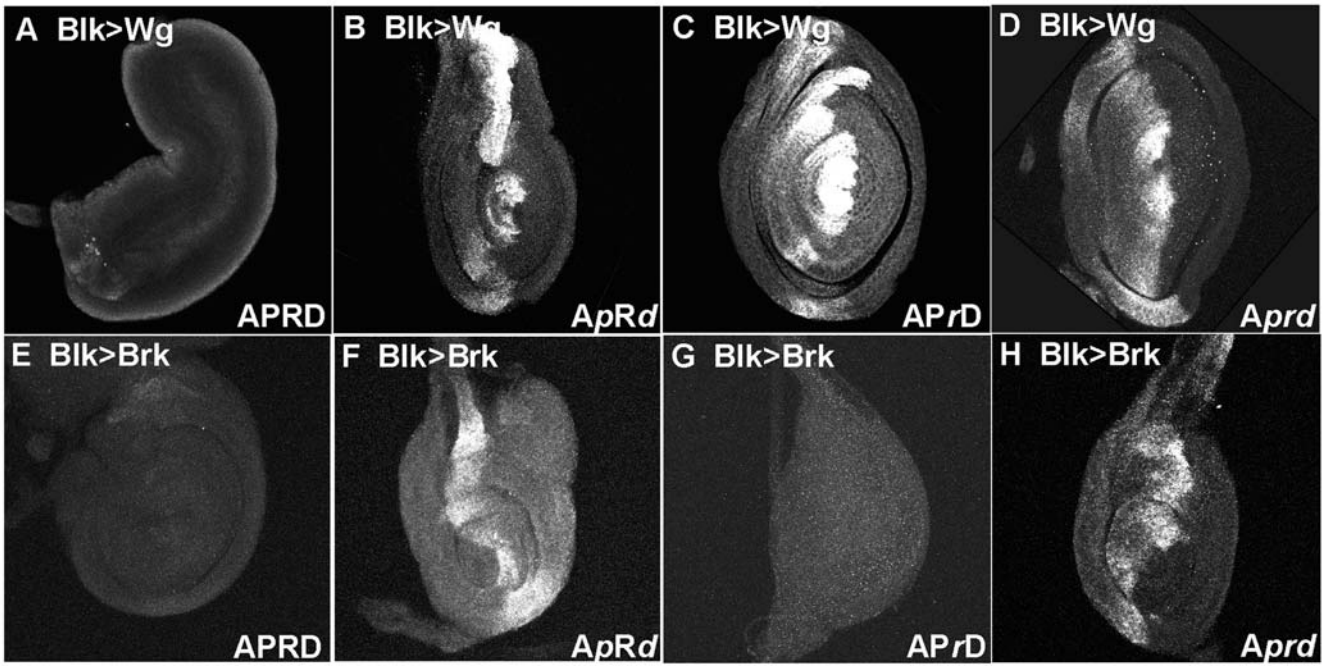

Figure 4. Simultaneous binding of BRK and dTCF is required for *dpp* repression.
A–H: 3rd instar leg imaginal discs. Dorsal is up and Anterior is to the left. A–D: response of *dpp* reporters to dpp^{blk} GAL4 driven expression of WG. E–H: response of *dpp* reporters to dpp^{blk} GAL4 driven expression of BRK. A: Ectopic dorsal expression of *wg* represses APRD>lacZ expression. B: Ectopic *wg* expression does not repress the APRD *dpp* reporter when all 5 of the dTCF binding sites are mutated (indicated by A*p*R*d*). C: WG expression does not repress the APRD *dpp* reporter when the BRK binding sites are mutated (AP*r*D). D: WG expression does not repress the APRD *dpp* reporter when all the dTCF and BRK binding sites are mutated (A*prd*). E: Ectopic dorsal expression of BRK represses APRD>lacZ expression. F: Ectopic BRK expression does not repress the APRD *dpp* reporter when all 5 of the dTCF binding sites are mutated (A*p*R*d*). G: Ectopic BRK expression does repress the *dpp* reporter when the BRK sites are mutated, APrD H: Ectopic BRK expression does not repress the *dpp* reporter when all the dTCF and BRK binding sites are mutated, A*prd*.
doi:10.1371/journal.pone.0000142.g004

anterior and posterior regions, and intermediate expression along the A/P boundary in the ventral leg disk [27–30].

To test whether BRK binds to both of the potential sites in the R region, we used surface plasmon resonance (SPR) with immobilized recombinant BRK protein in a DNA binding assay (Fig. 5A). The SPR sensogram shows that BRK can bind to the R region when at least one of the BRK binding sites is intact, but when both BRK sites are mutated, no binding is observed.

If BRK is specifically required for WG mediated repression of *dpp*, then introducing either or both mutations into the BRK sites (AP*rb1*D, AP*rb2*D, and AP*rb12*D) should lead to increased *dpp* expression in the ventral region of the leg disk. Indeed, mutation of either BRK site 1 or both sites, results in increased *dpp* expression that is restricted to the region of WG signaling (Fig. 5 B,C,D).

To determine whether BRK binding is an essential component of WG mediated *dpp* repression, we tested the ability of WG signaling to repress reporter constructs when the BRK sites are mutated. While ectopic *wg* expression is able to extinguish all APRD expression (Fig. 4A), ectopic WG cannot repress APRD when the BRK sites are mutated (AP*r*D) (Fig. 4C). Nor can ectopic WG suppress reporter gene expression when the dTCF sites are mutated (A*p*R*d*; Fig. 4B) or when both the dTCF and BRK sites are mutated (A*prd*) (Fig. 4D).

To investigate the interdependence of WG and BRK, we asked if BRK alone is sufficient to repress expression of the *dpp* reporter. Ectopic *brk* expression can repress intact APRD (Fig. 4E), but cannot repress APRD when the TCF sites are mutated (A*p*R*d*; Fig. 4F) indicating that BRK must synergize with TCF to repress *dpp* expression. Interestingly, high levels of ectopic BRK can repress APRD even when the BRK sites are mutated (AP*r*D; Fig. 4G) but only if the dTCF sites are intact (A*prd*; Fig. 4H; F). This suggests that under normal cellular conditions, loss of BRK binding sites prevents repressor complex formation but that experimental induction of high levels of BRK may allow repressor complexes to form that are anchored to the DNA by dTCF•ARM complexes. Taken together these data suggest that at normal factor concentrations both BRK and dTCF sites are necessary for WG mediated repression of *dpp* transcription but neither alone is sufficient.

DISCUSSION

Active Repression of *dpp* by WG defines a novel mode of WG mediated repression

TCF is emerging as a multifunctional transcriptional modulator that can act as both an activator and a repressor in multiple environments. In the absence of WNT signaling, LEF/TCFs become default repressors [4,31–33] of genes because they recruit co-repressors such as GRO and CtBP [13,34–36]. WNT signaling relieves this repression by causing β-catenin/ARM to accumulate in the nucleus and convert dTCF to a transcriptional activator, possibly by displacing or overriding the default co-repressor(s) [37]. This default repression can be further modulated by processes that antagonize the interaction of β-catenin with TCF.

Less well understood is the mechanism whereby TCF can repress genes in response to Wnt signaling. Expression of several genes is repressed in response to WNT signaling, including, *E-cadherin, dpp, Ubx, osteocalcin, stripe, svb, daughterless* [14–17,38–43].

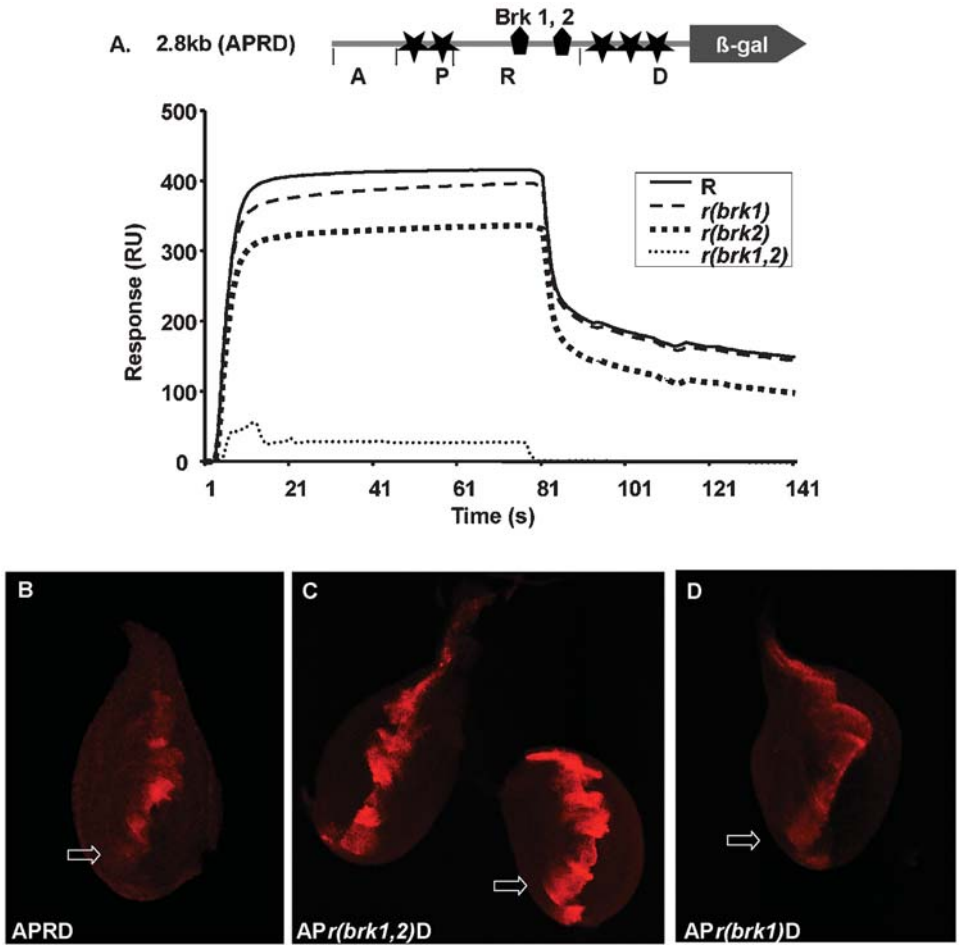

Figure 5. BRK binding is required to suppress *dpp* expression
BRK binding sites are located in the R domain of APRD (filled pentagons). SPR analysis shows BRK binding to the intact R domain (R). Mutation of BRK site 1 [*r(brk1)*] reduces binding incrementally, mutation of BRK site 2 [*r(brk2)*] reduces binding still further while mutation of both sites [*r(brk1,2)*] abolishes binding completely. The biophysical binding of BRK to its DNA sites correlates well with the biological responses caused by the same mutations. B: *dpp* expression is ventrally repressed in the intact APRD fragment (arrow). C: Mutation of both BRK sites leads to loss of repression and ventral expression of *dpp* (arrow). D: Mutation of a single BRK site leads to ventral expression of *dpp* (arrow).
doi:10.1371/journal.pone.0000142.g005

Thus far, one mechanism for WG/WNT dependent repression has been described namely, Competitive Repression [44]. In this case, dTCF represses gene activation by displacing other activating proteins through competition for the DNA binding site. For example, WG signaling represses *stripe* gene expression when dTCF binds to sites that overlap with the sites for the activator (CI) [15]. TCF has also been shown to mask the DNA binding domain of another transcription activator Runt and inhibit its binding to the osteocalcin promoter [42]. In both these cases, repression occurs in response to the WG/WNT signal and requires ARM. Here, we provide evidence of a second mechanism of WG/WNT directed repression, namely Direct Repression [44]. We show, for the first time, that WNT signaling can direct formation of a co-R•ARM•TCF complex that represses transcription. In the case of *dpp* repression, this co-R is BRK and the formation of a BRK•ARM•dTCF complex is required to actively repress *dpp* gene expression. Other genes, including *ovo/svb*, *da* and *dfz2* in Drosophila, are actively repressed by WG signaling and contain physically separated activating and repressing enhancer elements [12,14,38], but since the putative regulatory DNA regions necessary for repression of these genes have not been identified, it is not yet possible to tell if repression in these cases also requires an ARM•TCF complex.

Our studies show that BRK can interact with the dTCF•ARM complex to repress target genes. The behavior of the complex in response to altered levels of individual components, especially to altered levels of the non-DNA binding component, ARM, is not monotonic (e.g. repression is lost with both low and artificially high levels of ARM), suggesting a mechanism whereby both TCF and BRK can be titrated out by excess ARM which might be achieved by either direct or indirect interaction of ARM with both DNA binding components. Although, the specific molecular interactions that dictate the behavior of this complex remain to be determined, one can imagine several scenarios. To better understand the potential implications of these different scenarios, we constructed mathematical models that differ primarily in the nature of the interactions between DNA binding and non-binding components (Fig. S1–S5). This modeling analysis suggests distinct functional responses to different biochemical mechanisms that will be the subject of future studies. The biological responses described here and our analysis by modeling using reported values for the biophysical parameters [54–61], (Supporting Text S1; Figs. S1–S6

and Table S1) suggest a possible interaction mechanism in which a single ARM protein interacts either directly or indirectly with both TCF and BRK.

Since the *brk* gene appears to have no mammalian homolog, a different co-R could convert dTCF•ARM to a repressor complex in mammalian systems. The properties of this tri-partite repressor system are unique compared to the other known mechanisms of WG repression in that rather than being monotonic with respect to changes in all components, the system exhibits an optimum with respect to ARM levels. Systems with such properties tend to self-correct. For example, as ARM increases, *dpp* repression increases until ARM levels reach a point where they start to form non-productive complexes (e.g. increasing ARM positively feeds back on WG expression which coupled with less *dpp* allows greater levels of WG signaling and stabilized ARM). Higher levels of ARM will lead to the formation of non-productive complexes and squelching (Figs. S1Ci and S2; S5) and *dpp* repression will decline. Subsequent elevation of *dpp* expression will negatively affect WG signaling and ARM levels will correct back toward their optimum.

During development, it is essential for organ anlage such as imaginal discs in Drosophila or limb blastema in vertebrates, to develop the asymmetry required to produce a chiral appendage such as a leg. In imaginal discs, compartments of lineage restriction provide one axis of asymmetry along the A/P axis but no evidence for lineage restricted regions has been found in other axes such as the D/V axis of legs or antennae. How then are the dorsal and ventral territories defined and maintained? The system of mutual repression between Wg and Dpp described here, provides a mechanism for maintaining separate "territories" of *wg* and *dpp* expression in a developing field. Territories are regions of cells that are under the domineering influence of a particular morphogen and they differ from compartments in that they are not defined by lineage but are dynamically maintained by continuous morphogen signaling [11].

When targeted to an opposing morphogen gene (e.g. *dpp*), the properties of this novel BRK based co-repressor system contribute to a robust self organizing system that is capable of ensuring that territories of *wg* and *dpp* expression remain distinct and are maintained intact during the processes of growth and regeneration [10]; thus providing a molecular basis for the maintenance of such dynamic territories. Cross inhibition of morphogen expression may play a role in several developing systems including mammalian systems as similar repression of BMP by WNTs has been observed in the mammalian hair follicle and crypts of the developing gut [45].

MATERIALS AND METHODS

Drosophila melanogaster stocks and crosses

Genetic markers are described in Lindsay and Zimm [46]. Ectopic expression experiments employed the dpp^{blk}>Gal4 driver, P[GAL4-dpp.blk1 w+mW.hs]39B2/*TM6B* [26], and the HS>GAL4, P[GAL4-Hsp70.PB] driver mated to the following transgenes P[UAS>ARM52] (a kind gift of M. Peifer), P[UAS>dTCF] and P[UAS>DNdTCF] [22]. To enhance larval survival, animals were raised at low temperature until late 2nd/early 3rd instar and then shifted to 29°C. The dpp^{blink}>Gal4; UAS>dTCF animals were raised at 22°C and upshifted to 29°C for 3 h, 6 h, 12 h, 24 h and 48 h before dissection and staining of late 3rd instar imaginal discs. Similarly, dpp^{blink}>Gal4; UAS>DNdTCF animals were raised at 18°C and shifted to 25°C for 3 h, 6 h, 12 h and 24 h before dissection and staining. The crosses included various *dpp-lac*Z reporters as indicated in the text. For the dpp^{blk}>Gal4 crosses, balancers with *Green Flourescent Protein* (*GFP*) were used to identify larvae for dissection. The *dpp*>*lac*Z reporter lines used were BS3.0, BS3.1 (AP--), BS3.2 (--RD)(kind gifts from Ron Blackman; [19] as well as APRD, APR- and AP-D (Fig. 1A). The APRD construct is a 2.8 kb *Hind*III-*Nhe*I fragment that starts 2.6 kb 3′ from the beginning of BS3.0 (*i.e.* at co-ordinate 109.5). APR- is a 2.3 kb *Hin*d III-*Bsa* B1 fragment that has the same start point as APRD. The AP-D construct was generated by ligating a 525 bp *Ssp*I-*Nhe*I fragment containing three dTCF binding sites (co-ordinates 111.8–112.5) to the 5′ end of APRD cut with *Hind*III-*Ssp*I (Fig. 1A). APRD and BS3.0 expression were also monitored in a temperature sensitive *wg* background. The temperature sensitive *wg* allele, wg^{IL114} [23] was balanced with the compound balancer chromosome TSTL that has a translocation between the CyO and TM6B, *Tb* balancers. Homozygous mutant larvae were identified by the absence of a *Tubby* phenotype. The wg^{ts} mutant animals were raised at 18°C and shifted to 25°C for 24–48 hrs before dissection in late third instar.

Histochemistry

Imaginal discs were stained for β-galactosidase activity and mounted as described [7] with 2 minutes fixation. Expression was monitored in legs from at least 6 animals. The same changes in gene expression were observed in all animals with a particular genotype.

In situ hybridizations

wg and *dpp* expression were monitored by whole mount *in situ* hybridization using digoxigenin labeled antisense RNA probes prepared according to the manufacturer's specifications (Roche Molecular Biochemicals). Plasmids used were a 3 kb *wg* cDNA (wg651, a kind gift of B. Cohen) and a 4 kb *dpp* cDNA dppE55 [47] both in bluescript. Prehybridization and hybridization conditions are based on the protocol of Tautz and Pfeifle [48] with modifications [11].

Immunohistochemistry

Imaginal discs were fixed as for *in situs* and incubated overnight at 4°C with rabbit anti β-galactosidase antibody diluted 1:1000 with PBT (PBS+0.1% Triton×100)+3%BSA. A Cy3 or FITC conjugated donkey secondary antibody (Jackson Immunological Laboratory) was used at a 1/200 dilution. Images were analyzed on a Zeiss 510Meta confocal microscope. In each experiment, gene expression was monitored in legs from at least 6 animals each from 4 transgenic lines. The same changes in gene expression were observed in all animals with a particular genotype.

Protein Preparation and DNAse I footprinting

The DNA binding domain of dTCF was amplified by PCR using primers 5′CGCGGATCCGGAAGCAAAGCACACATCA, and 5′CGCGGATCCGCACCACTG ACTCTGTTG, and cloned into pET15b (Novagen). Bacterial extracts were prepared as described in [49]. Recombinant hLEF-1 [50] and dTCF were incubated with double-stranded DNA probes (5 to 15 fmol per reaction; single end-labeled on the 5′ end with [γ-^{32}P] ATP) for 1 minute on ice in a 50 µl reaction containing TM buffer (50 mM Tris pH 7.9, 12.5 mM $MgCl_2$, 1 mM EDTA, 20% glycerol, 0.1% NP-40, 50 mM KCl). DNase I work-up procedures are described in [51]. Human LEF-1 footprinted to the same sites as dTCF as expected from the highly similar DNA binding domains of these proteins [22]. All gels were analyzed with a PhosphorImager (Molecular Dynamics).

Mutation of dTCF and Brk binding sites

Site-directed mutants were made using the *Pfu* mutagenesis kit (Stratagene) with two complementary 30 nucleotide primers containing the new sequence. Approximately two-thirds of the colonies picked were the correct mutant. The sites were mutated as listed, wild type sequence is underlined, and mutated sequence is in capitals: (site 1) aacttctttcaa>aacttcttCGaa; (site 2) aacttcttcag>aacttcttCcag; (site 3) catcaatggcag>catTCatggcag; (site 4) gtacaaagaccc>gtaTGaagaccc; (site 5) tgccttttgatg>tgcctttATatg.

To mutate the BRK binding sites the following mutagenic oligonucleotides were used (the BRK site or its complement is shown with bold letters with the altered nucleotides underlined):

ggattcgggacctgaa**acgcc**atggatccccacgttcc>

ggattcgggacctgaaacATcatggatccccacgttcc

and

ggttttggggtttagtacca**ggcgt**caggtggctgaagcgtgag>

ggttttggggtttagtaccagATCtcaggtggctgaagcgtgag

The first mutation eliminates an *Nco*I site (ccatgg) while the second mutation creates a *Bgl*II site (agatct) making the detection of the mutations easier.

Surface Plasmon Resonance

Computational scanning of 2.8 kb APRD region revealed two consensus BRK binding sites. These were functionally confirmed by SPR on a Biacore 3000. Carboxymethylated dextran (CM5) coated sensor chips (Biacore AB, Uppsala, Sweden) were coated with 800 response units of anti-Flag antibody (Sigma) using NHS/EDC chemistry. HBS buffer (10 mM HEPES pH 7.4, 0.15 M NaCl, 3 mM EDTA, 0.005% (v/v) Surfactant P20; Biacore AB) was used as the running buffer with a flow rate of 10 µl/min. A fusion protein of the BRK-DNA binding domain with a FLAG epitope tag was purified [16] and captured onto the anti-Flag antibody. A 560 bp fragment spanning both putative BRK sites was tested for binding to immobilized BRK protein and binding was demonstrated. The role of the specific BRK sites was confirmed by mutating each site alone and both together within the context of the 560 bp fragment. Mutation of either BRK site reduced (slightly) but did not eliminate binding while mutation of both sites resulted in no detectable binding. The surface was regenerated with 2×5 µl of 30 mM HCl. The sensorgram for soluble antigen binding was corrected with the control buffer sensorgram

SUPPORTING INFORMATION

Supporting Text S1

Found at: doi:10.1371/journal.pone.0000142.s001 (0.82 MB DOC)

Table S1 Descriptions, values, and references of parameters used.

Found at: doi:10.1371/journal.pone.0000142.s002 (6.76 MB PDF)

Figure S1 Computational analysis activation/repression responses of wg and dpp under different possible modes of action A: Cartoon key for the 3 proteins and DNA binding sites involved. The wg enhancer (e3) serves to activate wg expression, while the dpp enhancer (e1e2) contains both TCF (e1) and BRK (e2) binding sites and is repressed by WG signaling. Both TCF and BRK bind DNA while ARM does not. B: (i) Depicts the TCF based activation complex formed at the wg enhancer (ii) depicts 3 possible models of complexes involving TCF, BRK and ARM that might contribute to repression. Model 1 requires concurrent binding of an ARM•dTCF complex and BRK but no physical interaction. Model 2 postulates that repression of dpp requires a bridge between TCF and BRK that requires ARM (bridging model). Model 3 proposes a direct binding between TCF and BRK. C(i) Examples of non-productive complexes that might form in the presence of high levels of A under the bridging model (1) or that might form in the presence of high levels of T in the direct binding model (2) (ii) examples of the possible sequences of binding events under model 1. There are several possible intermediates on the way to productive complexes (ATe3 or e1TABe2). D: The system is experimentally manipulated by increasing or decreasing the production rates (VT, VA, or VB) of T, A, or B. The computationally predicted response of wg activation (dashed line) and dpp repression (solid line) to changing levels of T, A or B expression is plotted over a wide range of production rates. The experimentally observed response of wild type dpp (e) and wg (f) expression to increased levels of ARM production (g, h) and TCF production (i, j) is shown in the bottom panels. The qualitative behavior predicted by the computational analysis disagrees with the concurrent binding and direct T•A binding models but is consistent with the bridging model when non-productive complexes are considered.

Found at: doi:10.1371/journal.pone.0000142.s003 (6.41 MB PDF)

Figure S2 All possible protein-protein and protein-DNA interactions for activation of wg and repression of dpp by models (1) and (2) are shown. Cartoons illustrate the interactions in question and the corresponding binding equations are listed to the right. A. Reactions leading to activation of wg are shown. B. Binding reactions for the concurrent binding model (model 1) are shown where the T•A complex does not bind B. C. Additional binding reactions describing events corresponding to the bridging model (model 2) are shown in a dashed box that correlates with equations in Fig. S3. These binding reactions together with those in B comprise the full set of reactions for the bridging model (2) without formation of NPCs. D. The binding reactions shown in the solid-box describe the formation of all possible NPCs. Together with the reactions shown in B and C, they comprise the full set of reactions for the bridging model with non-productive complexes. Transcriptionally active complexes are shown in bold.

Found at: doi:10.1371/journal.pone.0000142.s004 (6.24 MB PDF)

Figure S3 The equations governing activation and repression models (1) and (2) are shown. The unboxed, dash-boxed, and solid-boxed equations/terms correspond to the unboxed, dash-boxed, and solid-boxed interactions in Fig. S2. Model 1 (concurrent binding) is described by the set of equations not enclosed in the dashed and solid-boxes. Model 2 (ARM bridging) is described by the full set of equations. Omitting the terms in the solid-box describes the bridging model (2) in the absence of the formation of NPCs.

Found at: doi:10.1371/journal.pone.0000142.s005 (6.24 MB PDF)

Figure S4 All possible protein-protein and protein-DNA interactions for activation of wg and repression of dpp by the direct binding model (models 3) are shown. Several binding reactions in this model are possible intermediates enroute to final complexes and are identical to binding events shown for other models above.

A. Describes the wg activation reactions as in Fig. S2). B. Describes intermediate reactions that are the same as the concurrent binding reactions. C. Binding reactions unique to the T•B binding model are shown in the dashed box. D. The binding reactions leading to non-productive complexes in the T•B binding scenario are shown in the solid box. Transcriptionally active complexes are shown in bold.
Found at: doi:10.1371/journal.pone.0000142.s006 (6.24 MB PDF)

Figure S5 Equations governing repression by direct T•B binding (model 3) are shown. The complete set of equations describes the behavior of the direct T•B binding reactions in Fig. S4 with the inclusion of non-productive complexes. Omitting the terms in the solid-box describes the behavior under this model (3) in the absence of the formation of NPCs.
Found at: doi:10.1371/journal.pone.0000142.s007 (6.24 MB PDF)

Figure S6 Comparison of the response of T and B to increasing production rates. Why is the response to increased production rate of T to squelch T mediated regulation while increasing production rate of B has little effect? The lack of a known feedback on production of T leads to rapid change in the T:A ratio while the known feedback loops governing levels of B tend to maintain a steady ratio of B:A.
Found at: doi:10.1371/journal.pone.0000142.s008 (6.24 MB PDF)

ACKNOWLEDGMENTS

We are indebted to J. Munguia, T. Li, L. Banchik, S. Sanchez and M. Bahadori for excellent technical assistance, and to O. Marcu for critical reading of the manuscript. We thank Marc Peifer (Univ. North Carolina) for generously sharing stocks and information and K. Matthews and the National Drosophila Stock Center in Bloomington, IN for stocks. We also thank Ron Blackman for sharing flies and DNA constructs, which were used for this project

Author Contributions

Conceived and designed the experiments: JM TL HT AS MW. Performed the experiments: FW QN TL JP HT AS BN GS DI KG MW. Analyzed the data: JM FW QN TL JP HT AS BN GS DI KG MW. Wrote the paper: JM FW QN TL HT AS BN GS DI MW. Other: Designed and analyzed the computational model: FW QN DI GS BN.

REFERENCES

1. Behrens J, von Kries JP, Kuhl M, Bruhn L, Wedlich D, et al. (1996) Functional interaction of beta-catenin with the transcription factor LEF-1. Nature 382: 638–642.
2. Brunner E, Peter O, Schweizer L, Basler K (1997) pangolin encodes a Lef-1 homologue that acts downstream of Armadillo to transduce the Wingless signal in Drosophila. Nature 385: 829–833.
3. Cavallo R, Rubenstein D, Peifer M (1997) Armadillo and dTCF: a marriage made in the nucleus. Curr Opin Genet Dev 7: 459–466.
4. Riese J, Yu X, Munnerlyn A, Eresh S, Hsu SC, et al. (1997) LEF-1, a nuclear factor coordinating signaling inputs from wingless and decapentaplegic. Cell 88: 777–787.
5. Cadigan KM, Nusse R (1997) Wnt signaling: a common theme in animal development. Genes Dev 11: 3286–3305.
6. Brook WJ, Cohen SM (1996) Antagonistic interactions between wingless and decapentaplegic responsible for dorsal-ventral pattern in the Drosophila Leg. Science 273: 1373–1377.
7. Heslip TR, Theisen H, Walker H, Marsh JL (1997) Shaggy and dishevelled exert opposite effects on Wingless and Decapentaplegic expression and on positional identity in imaginal discs. Development 124: 1069–1078.
8. Jiang J, Struhl G (1996) Complementary and mutually exclusive activities of decapentaplegic and wingless organize axial patterning during Drosophila leg development. Cell 86: 401–409.
9. Johnston LA, Schubiger G (1996) Ectopic expression of wingless in imaginal discs interferes with decapentaplegic expression and alters cell determination. Development 122: 3519–3529.
10. Marsh JL, Theisen H (1999) Regeneration in insects. Semin Cell Dev Biol 10: 365–375.
11. Theisen H, Haerry TE, O'Connor MB, Marsh JL (1996) Developmental territories created by mutual antagonism between Wingless and Decapentaplegic. Development 122: 3939–3948.
12. Cadigan KM, Fish MP, Rulifson EJ, Nusse R (1998) Wingless repression of Drosophila frizzled 2 expression shapes the Wingless morphogen gradient in the wing. Cell 93: 767–777.
13. Fang M, Li J, Blauwkamp T, Bhambhani C, Campbell N, et al. (2006) C-terminal-binding protein directly activates and represses Wnt transcriptional targets in Drosophila. Embo J 25: 2735–2745.
14. Payre F, Vincent A, Carreno S (1999) ovo/svb integrates Wingless and DER pathways to control epidermis differentiation [see comments]. Nature 400: 271–275.
15. Piepenburg O, Vorbruggen G, Jackle H (2000) Drosophila segment borders result from unilateral repression of hedgehog activity by wingless signaling. Mol Cell 6: 203–209.
16. Saller E, Bienz M (2001) Direct competition between Brinker and Drosophila Mad in Dpp target gene transcription. EMBO Rep 2: 298–305.
17. Yang X, van Beest M, Clevers H, Jones T, Hursh DA, et al. (2000) decapentaplegic is a direct target of dTcf repression in the Drosophila visceral mesoderm. Development 127: 3695–3702.
18. Yost C, Farr GH 3rd, Pierce SB, Ferkey DM, Chen MM, et al. (1998) GBP, an inhibitor of GSK-3, is implicated in Xenopus development and oncogenesis. Cell 93: 1031–1041.
19. Blackman RK, Sanicola M, Raftery LA, Gillevet T, Gelbart WM (1991) An extensive 3′ cis-regulatory region directs the imaginal disk expression of decapentaplegic, a member of the TGF-beta family in Drosophila. Development 111: 657–666.
20. Masucci JD, Miltenberger RJ, Hoffmann FM (1990) Pattern-specific expression of the Drosophila decapentaplegic gene in imaginal disks is regulated by 3′ cis-regulatory elements. Genes Dev 4: 2011–2023.
21. Raftery LA, Sanicola M, Blackman RK, Gelbart WM (1991) The relationship of decapentaplegic and engrailed expression in Drosophila imaginal disks: do these genes mark the anterior-posterior compartment boundary? Development 113: 27–33.
22. van de Wetering M, Cavallo R, Dooijes D, van Beest M, van Es J, et al. (1997) Armadillo coactivates transcription driven by the product of the Drosophila segment polarity gene dTCF. Cell 88: 789–799.
23. Nusslein-Volhard C, Wieschaus E, Kluding H (1984) Mutations affecting the pattern of the larval cuticle in Drosophila Melanogaster. I. Zygotic loci on the second chromosome. Wilhelm Roux's Arch Dev Biol 193: 267–283.
24. Bryant PJ, Levinson P (1985) Intrinsic growth control in the imaginal primordia of Drosophila, and the autonomous action of a lethal mutation causing overgrowth. Dev Biol 107: 355–363.
25. Weinkove D, Neufeld TP, Twardzik T, Waterfield MD, Leevers SJ (1999) Regulation of imaginal disc cell size, cell number and organ size by Drosophila class I(A) phosphoinositide 3-kinase and its adaptor. Curr Biol 9: 1019–1029.
26. Staehling-Hampton K, Jackson PD, Clark MJ, Brand AH, Hoffmann FM (1994) Specificity of bone morphogenetic protein-related factors: cell fate and gene expression changes in Drosophila embryos induced by decapentaplegic but not 60A. Cell Growth Differ 5: 585–593.
27. Jazwinska A, Kirov N, Wieschaus E, Roth S, Rushlow C (1999) The Drosophila gene brinker reveals a novel mechanism of Dpp target gene regulation. Cell 96: 563–573.
28. Campbell G, Tomlinson A (1999) Transducing the Dpp morphogen gradient in the wing of Drosophila: regulation of Dpp targets by brinker. Cell 96: 553–562.
29. Minami M, Kinoshita N, Kamoshida Y, Tanimoto H, Tabata T (1999) brinker is a target of Dpp in Drosophila that negatively regulates Dpp-dependent genes. Nature 398: 242–246.
30. Muller B, Hartmann B, Pyrowolakis G, Affolter M, Basler K (2003) Conversion of an extracellular Dpp/BMP morphogen gradient into an inverse transcriptional gradient. Cell 113: 221–233.
31. Bienz M (1999) APC: the plot thickens. Curr Opin Genet Dev 9: 595–603.
32. Brannon M, Gomperts M, Sumoy L, Moon RT, Kimelman D (1997) A beta-catenin/XTcf-3 complex binds to the siamois promoter to regulate dorsal axis specification in Xenopus. Genes Dev 11: 2359–2370.
33. Roose J, Molenaar M, Peterson J, Hurenkamp J, Brantjes H, et al. (1998) The Xenopus Wnt effector XTcf-3 interacts with Groucho-related transcriptional repressors. Nature 395: 608–612.
34. Brantjes H, Roose J, van De Wetering M, Clevers H (2001) All Tcf HMG box transcription factors interact with Groucho-related co- repressors. Nucleic Acids Res 29: 1410–1419.
35. Cavallo RA, Cox RT, Moline MM, Roose J, Polevoy GA, et al. (1998) Drosophila Tcf and Groucho interact to repress Wingless signalling activity. Nature 395: 604–608.

36. Nusse R (1999) WNT targets. Repression and activation. Trends Genet 15: 1–3.
37. Barolo S, Posakony JW (2002) Three habits of highly effective signaling pathways: principles of transcriptional control by developmental cell signaling. Genes Dev 16: 1167–1181.
38. Cadigan KM, Jou AD, Nusse R (2002) Wingless blocks bristle formation and morphogenetic furrow progression in the eye through repression of Daughterless. Development 129: 3393–3402.
39. Conacci-Sorrell M, Zhurinsky J, Ben-Ze'ev A (2002) The cadherin-catenin adhesion system in signaling and cancer. J Clin Invest 109: 987–991.
40. Huber O, Korn R, McLaughlin J, Ohsugi M, Herrmann BG, et al. (1996) Nuclear localization of beta-catenin by interaction with transcription factor LEF-1. Mech Dev 59: 3–10.
41. Jamora C, DasGupta R, Kocieniewski P, Fuchs E (2003) Links between signal transduction, transcription and adhesion in epithelial bud development. Nature 422: 317–322.
42. Kahler RA, Westendorf JJ (2003) Lymphoid enhancer factor-1 and beta-catenin inhibit Runx2-dependent transcriptional activation of the osteocalcin promoter. J Biol Chem 278: 11937–11944.
43. Shimamura K, Hirano S, McMahon AP, Takeichi M (1994) Wnt-1-dependent regulation of local E-cadherin and alpha N-catenin expression in the embryonic mouse brain. Development 120: 2225–2234.
44. Levine M, Manley JL (1989) Transcriptional repression of eukaryotic promoters. Cell 59: 405–408.
45. Moore KA, Lemischka IR (2006) Stem cells and their niches. Science 311: 1880–1885.
46. Lindsley DL, Zimm GG (1992) The Genome of *Drosophila melanogaster*. San Diego: Academic Press.
47. Padgett RW, St Johnston RD, Gelbart WM (1987) A transcript from a Drosophila pattern gene predicts a protein homologous to the transforming growth factor-beta family. Nature 325: 81–84.
48. Tautz D, Pfeifle C (1989) A non-radioactive *in situ* hybridisation method for the localisation of specific RNAs in *Drosophila* embryos reveals translational control of the segmentation gene *hunchback*. Chromosoma 98: 81–85.
49. Prieve MG, Waterman ML (1999) Nuclear localization and formation of beta-catenin-lymphoid enhancer factor 1 complexes are not sufficient for activation of gene expression. Mol Cell Biol 19: 4503–4515.
50. Waterman ML, Fischer WH, Jones KA (1991) A thymus-specific member of the HMG protein family regulates the human T cell receptor C alpha enhancer. Genes Dev 5: 656–669.
51. Jones KA, Luciw PA, Duchange N (1988) Structural arrangements of transcription control domains within the 5′-untranslated leader regions of the HIV-1 and HIV-2 promoters. Genes Dev 2: 1101–1114.
52. Bergstrom DE, Merli CA, Cygan JA, Shelby R, Blackman RK (1995) Regulatory autonomy and molecular characterization of the Drosophila out at first gene. Genetics 139: 1331–1346.
53. St. Johnston RD, Hoffmann FM, Blackman RK, Segal D, Grimaila R, et al. (1990) Molecular organization of the decapentaplegic gene in Drosophila melanogaster. Genes Dev 4: 1114–1127.
54. Gill G, Ptashne M (1988) Negative effect of the transcriptional activator GAL4. Nature 334: 721–724.
55. Meyer ME, Gronemeyer H, Turcotte B, Bocquel MT, Tasset D, et al. (1989) Steroid hormone receptors compete for factors that mediate their enhancer function. Cell 57: 433–442.
56. Jazwinska A, Rushlow C, Roth S (1999) The role of brinker in mediating the graded response to Dpp in early Drosophila embryos. Development 126: 3323–3334.
57. Lee E, Salic A, Kruger R, Heinrich R, Kirschner MW (2003) The roles of APC and Axin derived from experimental and theoretical analysis of the Wnt pathway. PLoS Biol 1: E10.
58. Knapp S, Zamai M, Volpi D, Nardese V, Avanzi N, et al. (2001) Thermodynamics of the high-affinity interaction of TCF4 with beta-catenin. J Mol Biol 306: 1179–1189.
59. Lander AD, Nie Q, Wan FY (2002) Do morphogen gradients arise by diffusion? Dev Cell 2: 785–796.
60. Fall CP, Marland ES, Wagner JM, Tyson JJ (2002) Computational Cell Biology: Springer Verlag.
61. Eldar A, Shilo BZ, Barkai N (2004) Elucidating mechanisms underlying robustness of morphogen gradients. Curr Opin Genet Dev 14: 435–439.

Supporting Information for

Wingless Directly Represses DPP Morphogen Expression Via an Armadillo/TCF/Brinker Complex

Theisen et. al.

Theoretical exploration of the molecular interactions governing repression

Although many signaling pathways revert to a default repression state in the absence of signal [1], cooperative interactions that convert an activating WG signal into a repressing one have not been reported. Our experimental observations show that the response of the *dpp* system to changes in ARM levels is not monotonic; *dpp* repression is lost at both low and high levels of ARM. This raises the possibility of a novel interaction between the ARM•TCF complex and BRK.

To better understand how the biochemical interactions of these components might affect biological behavior, we decided to explore different scenarios for such a system *in silico*. We developed a series of ordinary differental equations (ODEs) to describe the possible interactions between two DNA binding proteins, a non-DNA binding protein and their DNA enhancer target sites $e_{1,2,3}$. Three mechanistic possibilities for their interaction were considered (Fig. S1B) and predicted behavior was compared with experimentally observed behavior. This analysis compared the behavior of an enhancer that positively responds to WG signaling such as the dTCF binding region of the *wg* enhancer that leads to *wg* activation (represented by e_3), with an enhancer (e_1e_2) that negatively responds to WG signaling such as the *dpp* repression region with dTCF binding sites (e_1) and BRK binding sites (e_2) (Fig. S1A). Binding of AT to e_3 activates *wg* (Fig. S1Bi), while repression of *dpp* requires A, T and B bound to e_1e_2 (Fig. S1Bii). To explore the dynamics of these possible systems, all possible molecular interactions were included without bias. Equilibria and rate constants derived from known measured values and known feedback loops are documented below.

We considered three possible models for the interaction of ARM, TCF and BRK in repressing *dpp* expression (Fig. S1): (1) In case 1, the concurrent binding model, an ARM•TCF complex and BRK bind DNA independently to cause repression but there is no physical interaction between them (Fig. S1Bii model1). (2) In case 2, the bridging model, ARM participates either directly or indirectly in forming a bridge that binds both BRK and TCF to

form a repressing complex e_1TABe_2 (Fig. S1Bii model2). In this scenario, ARM acts like a scaffold with at least 2 binding surfaces, one for TCF and one for BRK or for an intermediate that binds BRK. (3) In case 3, the direct T•B binding model, direct binding between BRK and dTCF occurs without the participation of a non-DNA binding element (Fig. S1Bii model 3). These putative interactions do not exclude the possibility of additional elements, but the major distinction between the three scenarios is whether independent DNA binding elements interact directly or whether a non-DNA binding bridge is required.

The response of *wg* and *dpp* to varying levels of ARM, TCF and BRK, was analyzed in the context of each of the 3 mechanistic models. One modeling scenario allowed all possible mass action binding events, which permits the formation of non-productive complexes (NPCs; Fig. S1Ci), while a second scenario eliminated the formation of non-productive complexes (NPCs). The modeling predicted different experimental responses for each of the different mechanisms (Fig. S1D), with the most prominent distinction being the response of activation and repression to excess levels of ARM and dTCF.

This analysis demonstrates that different formalized mechanisms of repression can be distinguished by the response of the system to changes in the levels of components and in this case changes in the levels of non-DNA binding components (e.g. ARM) provide the distinguishing behaviors. Experimentally we observe that over-expression of ARM (using Blk>Gal4 to drive UAS>ARM in a D/V stripe in the leg imaginal disc) causes both the APRD *dpp* reporter gene and endogenous *dpp* mRNA (Fig. S1G; data not shown) expression to expand into the ventral region of the leg disc. Endogenous *wg* mRNA expression (Fig. S1H) remains on in the ventral region but expands into the dorsal territory in these animals. Thus, over-expression of ARM activates WG target genes (e.g. *wg*) but squelches WG dependent repression. This squelching behavior [2] can help distinguish between biochemical mechanisms that depend only on the DNA binding components versus mechanisms in which a non-DNA binding component forms a bridge between the two DNA binding species [3,4] (Fig. S1Bii2). For example, direct binding between TCF and BRK predicts increased repression with increasing ARM (Fig. S1Dd), while models that do not include ARM•BRK or TCF•BRK interaction predict no change in repression upon increased ARM. Responses of the system to experimental changes in TCF and BRK levels also support a bridging model. For example, models that fail to include ARM•BRK binding or models that do not permit the formation of non-productive complexes, fail to

anticipate the loss of repression seen with excess TCF. The reduced sensitivity of *dpp* repression to changes in BRK levels compared to changes in TCF levels also supports a bridging model. Both the experimentally observed changes in gene expression and the computational analysis suggest a possible bridging mechanism (Fig. S1Biib) for ARM, TCF and BRK mediated repression.

Materials and Methods

A series of ODEs describe the possible binding of A to T, A to B, B to T and T and B to their respective enhancers on the DNA ($e_{1,\ 2\ \text{or}\ 3}$) (the complete set of ODEs is shown in Figs. S2-5) and these were used to explore different possible mechanisms of action of this system. We adopted the following abbreviations simplicity in the computational analysis: WG = W; DPP = D; ARM = A; dTCF = T; and BRK = B. dTCF binding sites in the *dpp* gene are represented by e_1 and BRK enhancer binding sites by e_2 and dTCF binding sites in the *wg* gene are represented by e_3 (Fig. S1A). These expressions incorporate variables for synthesis ($V_{T,\ A\ \text{or}\ B}$) and degradation of the components (K_{deg}).

The concentrations of A and B are governed by feedback loops. To mimic the stabilization of ARM in response to WG signaling, the regulation of A which is governed by the degradation of ARM, $K_{degA,}$ is described by an equation in which A is constantly degraded but stabilized by WG signaling (i.e. increasing ATe_3). $K_{\deg A} = K_{A\min} + \dfrac{K_{A\max} - K_{A\min}}{1 + \left[\dfrac{ATe_3}{\gamma_A}\right]^m}$

The Hill coefficient (m) imparts cooperativity to the interaction and gamma is a term that reflects the sensitivity of the system to feedback regulation.

To mimic repression of *brk* by DPP [5-7], decreasing D (increasing e_1TABe_2), has a positive feedback on the production of B (V_B), represented by,

$$V_B = V_{B\min} + \frac{\left(V_{B\max} - V_{B\min}\right)\left(e_1 TABe_2\right)^n}{\gamma_B^n + \left(e_1 TABe_2\right)^n}$$

where V_B is the production rate of BRK, γ is the signaling sensitivity or EC50, the effective concentration so that maximal feedback occurs at the halfway point between the maximum and minimum response values, *m* and *n* are the Hill coefficients that provide a measure of the extent of cooperativity in binding, K_{Amax} and K_{Amin} are maximum and minimum degradation rates of

ARM, and V_{Bmax} and V_{Bmin} are maximum and minimum production rates of BRK. ARM has a constant production rate denoted by V_A. To preserve the conservation of T as experimentally observed in the ventral leg disc cells, T is governed by a production rate (V_T) and a degradation rate ($K_{degT} = V_T/T$). To explore parameters, all molecules are allowed to interact randomly in any order with no bias.

Using these molecules, we modeled WG directed *dpp* repression and *wg* activation. To model repression, we consider three possible modes of ARM, TCF and BRK interactions (Fig. S1Bii): (1) An ARM•TCF complex binds to e_1 and BRK binds e_2 concurrently to cause repression (ATe_1e_2B) but there is no physical interaction between ARM and BRK. (2) ARM can form a bridge between the two DNA binding elements, BRK and TCF, to form a repressing complex e_1TABe_2 (this bridge may involve other intermediate molecules). (3) BRK and dTCF directly associate with each other. For each model, we examine the behavior with and without formation of nonproductive complexes (NPCs) that compete (squelch) nonlinearly with the formation of the repressing complex [2,3]. To model autoactivation of *wg*, we define a functional activation complex as ARM·TCF bound to *e3*. The values of and references for the parameters used are given in Table 1. Average values are used for unknown parameters. We define a cooperative interaction to be the final step in the formation of a tripartite complex where 2 parts are already bound facilitating the formation of the last interaction. For example, if A•T is bound at e_1 and B is bound at e_2, this will facilitate the interaction between A and B to form the functional complex in Case 2. The association rates for the cooperative interactions are ten times faster than normal interactions. The binding reactions for activation and repression under models 1 and 2 are described in Fig. S2. The full set of equations used to describe these are presented in Fig. S3 and the parameters used are described in Table I. Binding reactions and equations for repression model 3 (direct T•B binding) are shown in Fig. S4 and S5 respectively.

Results:

Exploring three possible modes of repression by TCF, ARM and BRK

We tested 3 different scenarios for repression. We first explored a concurrent binding model in which A•T and B sites are occupied simultaneously but with no physical interaction between B and the A•T complex (Fig. S1B). If all components are allowed to interact in any

order with no bias, this model is described by eleven non-linear ODEs (Fig. S2; S3). To mimic the *in vivo* over-expression of A, B, and T respectively, the formation of a functional repression complex is plotted for 3 cases: when V_A is varied from 10^{-7} to 10^{-1} μM/s, when V_B is varied from10^{-4} to 10^{-1} μM/s and when V_T is varied from 10^{-5} to 10^{-3} μM/s. In agreement with experimental observation, this case predicts that the amount of functional repression complex formed increases with increasing V_B (Fig. S1De), while the amount of repression complex is predicted to decrease with increasing V_T (Fig. S1Df).

Next, we explored a scenario where there is physical contact between T bound at e_1 and B bound at e_2 that involves a bridge which includes A to form a functional repression complex (Fig. S1). This model demands that A has 2 protein binding surfaces (namely A binds T (directly as is known) and B (either directly or via intermediates). Changes in the relative amounts of A, B, and T determine whether productive repression complexes or non-productive complexes form. An example of the type of non-productive complex that can form is a complex where AT is bound at e_1 and AB is bound at e_2, thus preventing the formation of the bridge between T and B (Fig. 6Ci). This system is described by 27 ODEs (Fig. S2; S3). If non-productive complexes are excluded from the system, repression increases with increasing V_A (10^{-7}–10^{-4} μM/s), V_B (10^{-4}–10^{-1}) (Fig. S1Db) but decreases with increasing V_T (10^{-5} to 10^{-3} μM/s; Fig. S1Dj). When non-productive complexes are included in the system, repression complex formation increases at low values of V_A (10^{-7}–10^{-4} μM/s) and decreases at higher values (10^{-4}–10^{-1} μM/s) as observed experimentally. In addition, repression is still directly related to changes in V_B and inversely related to changes in V_T. Thus, the bridging model (Fig. S1Bii2) with NPCs included is consistent with all experimental observations.

We also explored a third scenario where T and B interact with each other directly and A still binds to T (Fig. S4; S5). NPCs can form in this system too (Fig. S1Biii3), for example A•T can bind at e_1 and free T can bind to B at e_2 thus preventing the interaction of DNA bound T and B. When non-productive complexes are included, repression complex formation is directly related to changes in A (Fig. S1Dd) and B (Fig. S1Dh) and inversely related to changes in T (Fig. S1Dl). Thus, this model mimics *in vivo* observations for changes in T and B but is inconsistent with the changes observed when A is over-expressed.

The results obtained from exploring these different scenarios suggest that formation of NPCs is a crucial component of this system's behavior and thus, we focus on the T•A•B bridging model (Fig. S1Bii2) with formation of NPCs in the analyses below.

Modeling of wg activation by TCF and ARM

Modeling of *wg* expression in the ventral leg disc in response to WG signaling requires that an ARM•TCF complex bind to the *wg* DNA enhancer binding site e_3. Thus, *wg* expression is a reflection of the formation of the ATe_3 complex. The possible interactions involved in formation of ATe_3 and the corresponding governing equations are shown in Fig. S3; S3). The computational analysis agrees with the experimental result that over-expression of ARM promotes higher level of *wg* expression. The dashed curves in Fig. S1Da-d show that increasing ARM production rate also increases computationally predicted *wg* expression to a plateau at 100% activation, which is consistent with the experimental observation. In contrast, increasing the production rate of T causes a decrease in the formation of ATe_3, a functioning activation complex. Again this mimics experimental observations. Thus the computational model mimics the effects of excess ARM and TCF on *wg* expression

Discussion

Computational modeling can provide a powerful complement to experimental manipulations that can inform and complement our understanding of biological observations. Modeling of the cytosolic events triggered by Wnt signaling has been used to reveal mechanisms of signal transduction and to identify critical targets that regulate the system and thus represent potentially excellent targets for therapeutic intervention [8]. Here we focus on events inside the nucleus, specifically the less well understood process of Wg-dependent repression.

An ARM bridging model faithfully accounts for all aspects of the system behavior

Manipulations of ARM, TCF and BRK levels *in vivo* elicit different changes in *wg* and *dpp* expression. Of the 3 models tested, only the bridging model mimics all the experimental observations (Fig. S1). The effect of altered levels of TCF on *dpp* repression are quite different in the different models. Model (1) and (2) without NPCs show that level of *dpp* repression is

insensitive to changes in TCF concentration (Fig. S1Di, j) while both the bridging model with NPCs (model 2) and model (3) show the same trend of decreasing repression with increasing TCF as is observed experimentally. In contrast and in agreement with experimental observation, both *wg* activation and *dpp* repression are relatively insensitive to changing levels of BRK under all scenarios (Fig. S1De-h). The response to altered levels of ARM is the key distinguishing feature among the mechanistic models. We conclude that the response of *dpp* repression to altered levels of A, T and B suggests a mechanism which involves the bridging of ARM between dTCF and BRK which bind to e_1 and e_2 respectively and the formation of NPCs.

The results obtained from exploring these scenarios suggest that the formation of NPCs is a critical component of the system's behavior. These complexes provide a mechanism for squelching by over-expression of a non-DNA binding protein [3].

dTCF is directly required for activation of WG targets (*e.g*. Ubx; [9]) and for the default repression of genes in the absence of WG. Counter to expectation, excess dTCF interferes with WG autoactivation in the ventral leg (Fig. S1Dl). Modeling suggests that as the amount of free T increases, the ratio of T to AT increases such that there is a greater likelihood of forming Te_3 than A•Te_3 complexes. Excess T also interferes with WG directed repression. As described above, it causes the formation of non-productive repression complexes (Fig. S1Ci) that leads to loss of *dpp* repression (Fig. S1Dk), which in turn antagonizes *wg* activation. Although the response to altered dTCF levels is similar for several of the models, the faithful prediction of this non-intuitive behavior further validates the model.

The effect of altered BRK levels

Unlike TCF, the response of the system to changes in levels of BRK is much is slower. Analysis suggests that any dominant negative effect in response to elevated BRK would require considerably higher levels of BRK than TCF. Why do excess TCF and BRK levels predict different outcomes? Increasing TCF reduces ATe_3 formation. Decreased ATe_3 correlates with decreased WG signaling which leads to increased ARM degradation. Thus as T increases, A decreases causing the T:A ratio to rapidly increase (Fig. S6). With a large excess of free T, there is a greater chance that free T rather than AT will bind at e_3. In contrast, increasing BRK production rate does not feed back on ARM degradation, thus the B:A ratio does not show a measurable change over the range of BRK production tested. Thus the relative concentrations

of A, B and T are such that as B increases, more productive complexes can form on e_1e_2. For instance, an increase of V_T from 10^{-4} to 10^{-3} μM decreases the ratio A to T by two orders of magnitude (0.0249 to 0.00065). However, varying V_B by the same value only results a decrease of the same order of magnitude in the A to B ratio (from 93.2 to 9.318). This inter-related chain of interactions results in a close to normal ARM to BRK ratio. Thus, while the squelching effects of excess dTCF affect both *wg* and *dpp* and lead to an increasing cascade of ARM lowering events, the response to increasing BRK leads to a dampening effect that is consistent with the observation that demonstrable changes in the level of repression are not observed in tissues in response to levels of elevated BRK that are achievable experimentally.

Summary

Our interpretation of experimental results and testing by computational modeling, suggest the following. (1) A two component system with one DNA binding element (e.g.T) and one non-DNA binding element (e.g. A), such as the ARM•dTCF system that activates *wg*, behaves monotonically with respect to altered concentrations of the non-DNA binding component. The ratio of the nonDNA binding to DNA binding components (A:T) is important. At any fixed concentration of T, increasing A, increases wg activation (ATe_3), which further increases A due to feedback. However, when T is increased at a fixed concentration of A, active DNA bound complexes increase until the T:A ratio causes free T to compete with AT for DNA binding, at which point ATe_3 formation and thus *wg* activation, decreases.

A system that involves 2 distinct DNA binding components, such as the repression system for *dpp*, can be similarly analyzed. If the two DNA binding components act independently or if they physically interact directly with each other, the level of productive complex on the DNA behaves monotonically with respect to changes in the non-DNA binding component concentration. On the other hand, if there is physical interaction between the two DNA binding components that is mediated through a non-DNA binding component (e.g. such as ARM and possibly additional components) the system reflects a bimodal response to changes in the concentration of the non-DNA binding component(s). This leads to a self-correcting tendency of the system in response to changing levels of the bridging elements (e.g. ARM). Our experimental manipulations demonstrate that a robust self organizing system of morphogen regulation is operative in leg imaginal discs and the theoretical explorations described here

support the view that the three component system involving two DNA binding elements interacting with a non-DNA-binding component (BRK•ARM•dTCF) is unique in accounting for the observed behavior of the system to experimental manipulation.

Supporting Information: Figure legends

Figure S1. Computational analysis activation/repression responses of *wg* and *dpp* under different possible modes of action

A: Cartoon key for the 3 proteins and DNA binding sites involved. The *wg* enhancer (e_3) serves to activate *wg* expression, while the *dpp* enhancer (e_1e_2) contains both TCF (e_1) and BRK (e_2) binding sites and is repressed by WG signaling. Both TCF and BRK bind DNA while ARM does not. **B:** (i) Depicts the TCF based activation complex formed at the *wg* enhancer (ii) depicts 3 possible models of complexes involving TCF, BRK and ARM that might contribute to repression. Model 1 requires concurrent binding of an ARM•dTCF complex and BRK but no physical interaction. Model 2 postulates that repression of *dpp* requires a bridge between TCF and BRK that requires ARM (bridging model). Model 3 proposes a direct binding between TCF and BRK. **C**(i) Examples of non-productive complexes that might form in the presence of high levels of A under the bridging model (1) or that might form in the presence of high levels of T in the direct binding model (2) (ii) examples of the possible sequences of binding events under model 1. There are several possible intermediates on the way to productive complexes (ATe_3 or e_1TABe_2). **D:** The system is experimentally manipulated by increasing or decreasing the production rates (V_T, V_A, or V_B) of T, A, or B. The computationally predicted response of *wg* activation (dashed line) and *dpp* repression (solid line) to changing levels of T, A or B expression is plotted over a wide range of production rates. The experimentally observed response of wild type *dpp* (e) and *wg* (f) expression to increased levels of ARM production (g, h) and TCF production (i, j) is shown in the bottom panels. The qualitative behavior predicted by the computational analysis disagrees with the concurrent binding and direct T•B binding models but is consistent with the bridging model when non-productive complexes are considered.

Figure S2 All possible protein-protein and protein-DNA interactions for activation of *wg* and repression of *dpp* by models (1) and (2) are shown.

Cartoons illustrate the interactions in question and the corresponding binding equations are listed to the right. **A.** Reactions leading to activation of *wg* are shown. **B.** Binding reactions for the concurrent binding model (model 1) are shown where the T•A complex does not bind B. C. Additional binding reactions describing events corresponding to the bridging model (model 2) are shown in a dashed box that correlates with equations in Fig. S3. These binding reactions

together with those in B comprise the full set of reactions for the bridging model (2) without formation of NPCs. **D.** The binding reactions shown in the solid-box describe the formation of all possible NPCs. Together with the reactions shown in B and C, they comprise the full set of reactions for the bridging model with non-productive complexes. Transcriptionally active complexes are shown in bold.

Figure S3. The equations governing activation and repression models (1) and (2) are shown.

The unboxed, dash-boxed, and solid-boxed equations/terms correspond to the unboxed, dash-boxed, and solid-boxed interactions in Fig. S2. Model 1 (concurrent binding) is described by the set of equations not enclosed in the dashed and solid-boxes. Model 2 (ARM bridging) is described by the full set of equations. Omitting the terms in the solid-box describes the bridging model (2) in the absence of the formation of NPCs.

Figure S4. All possible protein-protein and protein-DNA interactions for activation of *wg* and repression of *dpp* by the direct binding model (models 3) are shown.

Several binding reactions in this model are possible intermediates enroute to final complexes and are identical to binding events shown for other models above. A. Describes the *wg* activation reactions as in Fig. S2). B. Describes intermediate reactions that are the same as the concurrent binding reactions. C. Binding reactions unique to the T•B binding model are shown in the dashed box. D. The binding reactions leading to non-productive complexes in the T•B binding scenario are shown in the solid box. Transcriptionally active complexes are shown in bold.

Figure S5. Equations governing repression by direct T•B binding (model 3) are shown.

The complete set of equations describes the behavior of the direct T•B binding reactions in Fig. S4 with the inclusion of non-productive complexes. Omitting the terms in the solid-box describes the behavior under this model (3) in the absence of the formation of NPCs.

Figure S6. Comparison of the response of T and B to increasing production rates.

Why is the response to increased production rate of T to squelch T mediated regulation while increasing production rate of B has little effect? The lack of a known feedback on production of

T leads to rapid change in the T:A ratio while the known feedback loops governing levels of B tend to maintain a steady ratio of B:A.

Table 1 Descriptions, values, and references of parameters used.

Symbol	Description	Value and unit	Justification
l_+	DNA-protein association rate	$2.22\times10^{-2}\ \mu M^{-1}\ \sec^{-1}$	Preliminary data from SPR analysis
l_-	DNA-protein dissociation rate	$4.11\times10^{-5}\ \sec^{-1}$	Preliminary data from SPR analysis
k_+	protein-protein association rate	$1.01\times10^{-1}\ \mu M^{-1}\ \sec^{-1}$	[10]
k_-	protein-protein dissociation rate	$8.47\times10^{-4}\ \sec^{-1}$	[10]
V_A V_T V_{Bmax} V_{Bmin}	production rate of ARM Production rate of TCF Maximum production rate of BRK Minimum production rate of BRK	$10^{-7}-10^{-1}\ \mu M\ \sec^{-1}$ $10^{-5}-10^{-3}\ \mu M\ \sec^{-1}$ $10^{-4}-10^{-1}\ \mu M\ \sec^{-1}$ $10^{-6}-10^{-3}\ \mu M\ \sec^{-1}$	Covers wide range of production where minimum corresponds to endogenous expression and maximum corresponds to over-expression via Gal4 activation
K_{Amax} K_{Amin}	maximum and minimum degradation rates of ARM	$10^{-2}\ \sec^{-1}$ $10^{-4}\ \sec^{-1}$	Covers wide range where maximum degradation results in no accumulation of Arm (no WG signaling) and minimum degradation mimics WG signaling.
K_{degB}	Degradation rate of BRK	$10^{-3}\ \sec^{-1}$	Rate of degradation computed from production rate and initial value of BRK to achieve steady state
γ_A γ_B	EC_{50}, effective concentration at 50% (1) for feedback of *wg* activation on degradation of A (2) for feedback of *dpp* repression on production of B	$10^{-2}-10^{-4}\ \mu M$	Values of gammas are chosen so that maximal feedback occurs at the halfway point between the maximum and minimum response values.
m and *n*	Hill coefficients	1	Hill coefficient of one is commonly used to allow a plausible rate of transition from maximum to minimum values e.g. [11,12]
$(e_1e_2)_0$	total DNA binding sites for repression	$10^{-3}\ \mu M$	Value corresponds to 2 sites /cell. Cell volume from [13]
$(e_3)_0$	total DNA binding sites for activation	$10^{-3}\ \mu M$	Value corresponds to 2 sites /cell. Cell volume from [13]
f_1 and f_2	cooperative association and dissociation factors	10 and 1	Reflects cooperative interactions occurring 10 fold faster than non cooperative reactions

Legend: A brief description of each of the parameters used in modeling is given along with range of values used and references that validate those values.

Literature cited:

1. Barolo S, Posakony JW (2002) Three habits of highly effective signaling pathways: principles of transcriptional control by developmental cell signaling. Genes Dev 16: 1167-1181.
2. Gill G, Ptashne M (1988) Negative effect of the transcriptional activator GAL4. Nature 334: 721-724.
3. Levine M, Manley JL (1989) Transcriptional repression of eukaryotic promoters. Cell 59: 405-408.
4. Meyer ME, Gronemeyer H, Turcotte B, Bocquel MT, Tasset D, et al. (1989) Steroid hormone receptors compete for factors that mediate their enhancer function. Cell 57: 433-442.
5. Jazwinska A, Rushlow C, Roth S (1999) The role of brinker in mediating the graded response to Dpp in early Drosophila embryos. Development 126: 3323-3334.
6. Campbell G, Tomlinson A (1999) Transducing the Dpp morphogen gradient in the wing of Drosophila: regulation of Dpp targets by brinker. Cell 96: 553-562.
7. Minami M, Kinoshita N, Kamoshida Y, Tanimoto H, Tabata T (1999) brinker is a target of Dpp in Drosophila that negatively regulates Dpp-dependent genes. Nature 398: 242-246.
8. Lee E, Salic A, Kruger R, Heinrich R, Kirschner MW (2003) The roles of APC and Axin derived from experimental and theoretical analysis of the Wnt pathway. PLoS Biol 1: E10.
9. Riese J, Yu X, Munnerlyn A, Eresh S, Hsu SC, et al. (1997) LEF-1, a nuclear factor coordinating signaling inputs from wingless and decapentaplegic. Cell 88: 777-787.
10. Knapp S, Zamai M, Volpi D, Nardese V, Avanzi N, et al. (2001) Thermodynamics of the high-affinity interaction of TCF4 with beta-catenin. J Mol Biol 306: 1179-1189.
11. Lander AD, Nie Q, Wan FY (2002) Do morphogen gradients arise by diffusion? Dev Cell 2: 785-796.
12. Fall CP, Marland ES, Wagner JM, Tyson JJ (2002) Computational Cell Biology: Springer Verlag.
13. Eldar A, Shilo BZ, Barkai N (2004) Elucidating mechanisms underlying robustness of morphogen gradients. Curr Opin Genet Dev 14: 435-439.

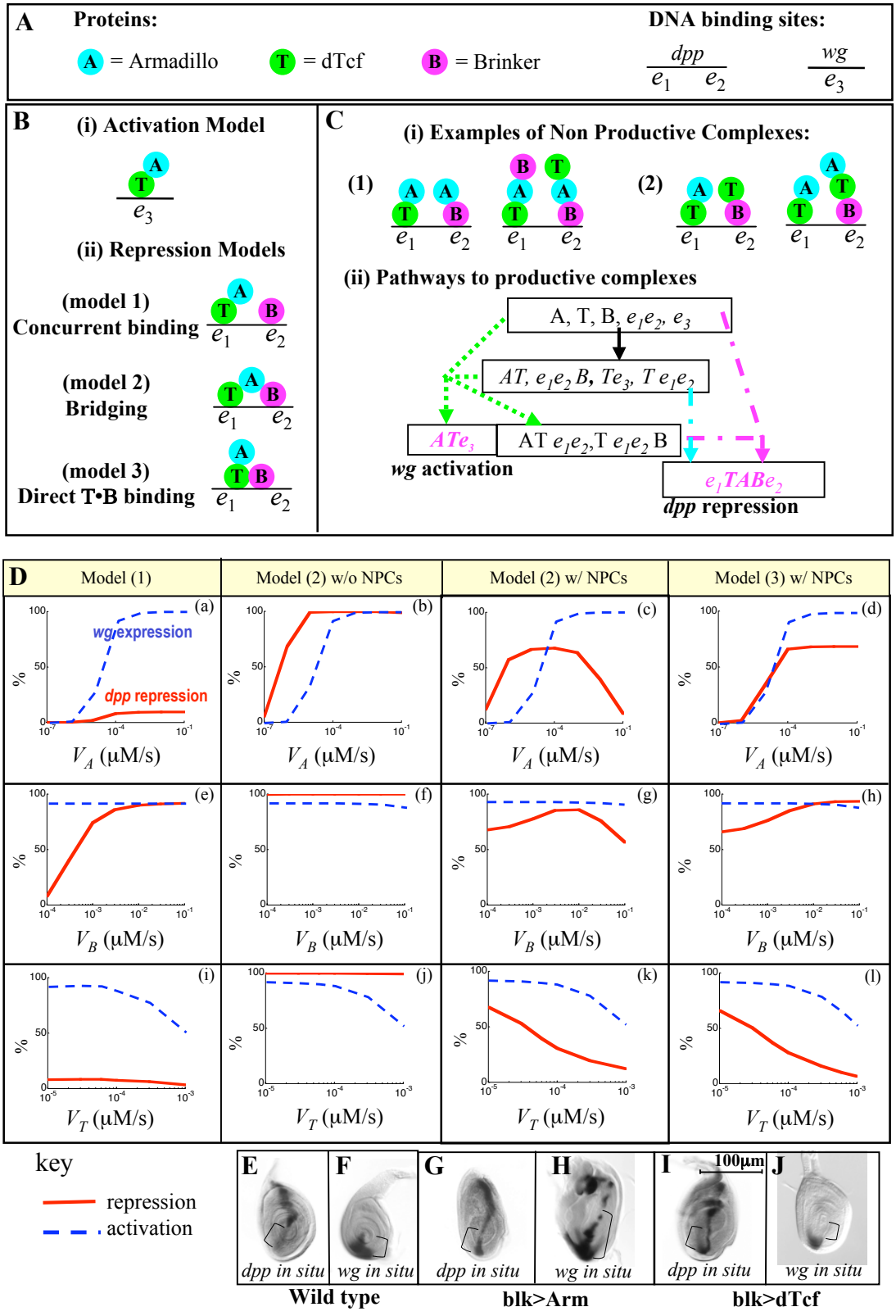
A
Proteins:
A = Armadillo
T = dTcf
B = Brinker
DNA binding sites:
dpp
e1 e2
wg
e3
B
(i) Activation Model
(ii) Repression Models
(model 1)
Concurrent binding
(model 2)
Bridging
(model 3)
Direct T•B binding
C
(i) Examples of Non Productive Complexes:
(1)
(2)
(ii) Pathways to productive complexes
A, T, B, e1e2, e3
AT, e1e2 B, Te3, T e1e2
ATe3
AT e1e2,T e1e2 B
wg activation
e1TABe2
dpp repression
D
Model (1)
Model (2) w/o NPCs
Model (2) w/ NPCs
Model (3) w/ NPCs
wg expression
dpp repression
VA (μM/s)
VB (μM/s)
VT (μM/s)
key
repression
activation
E
F
G
H
I
J
100μm
dpp in situ
wg in situ
Wild type
blk>Arm
blk>dTcf

Descriptions of reactions for activation and repression models 1;2 described in Fig S1.

A. *wg* activation reactions (see Fig S1Bi)

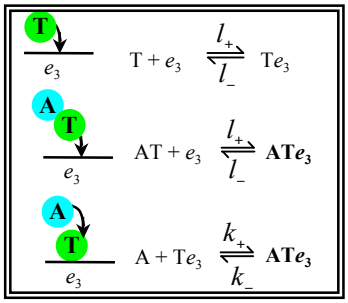

B. Model 1, Concurrent binding reactions (No A-B or T-B binding) (see Fig S1Bii)

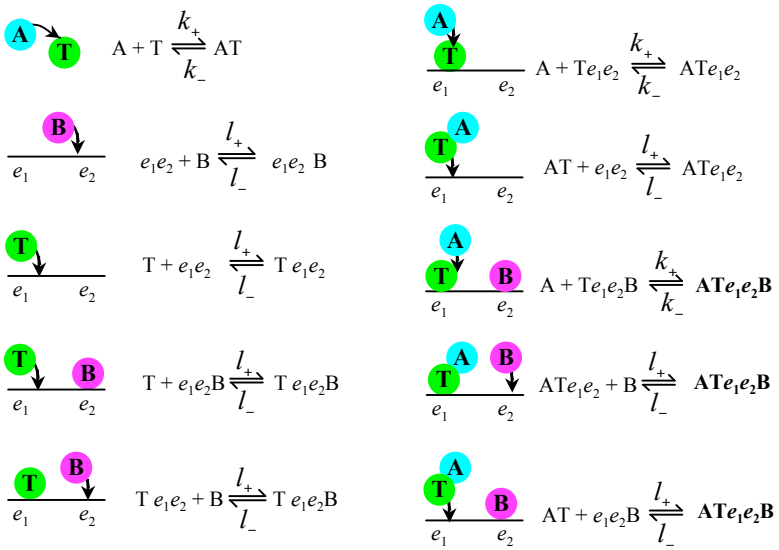

C. Model 2, Reactions leading to productive complexes in ARM bridging model (A-B binding)

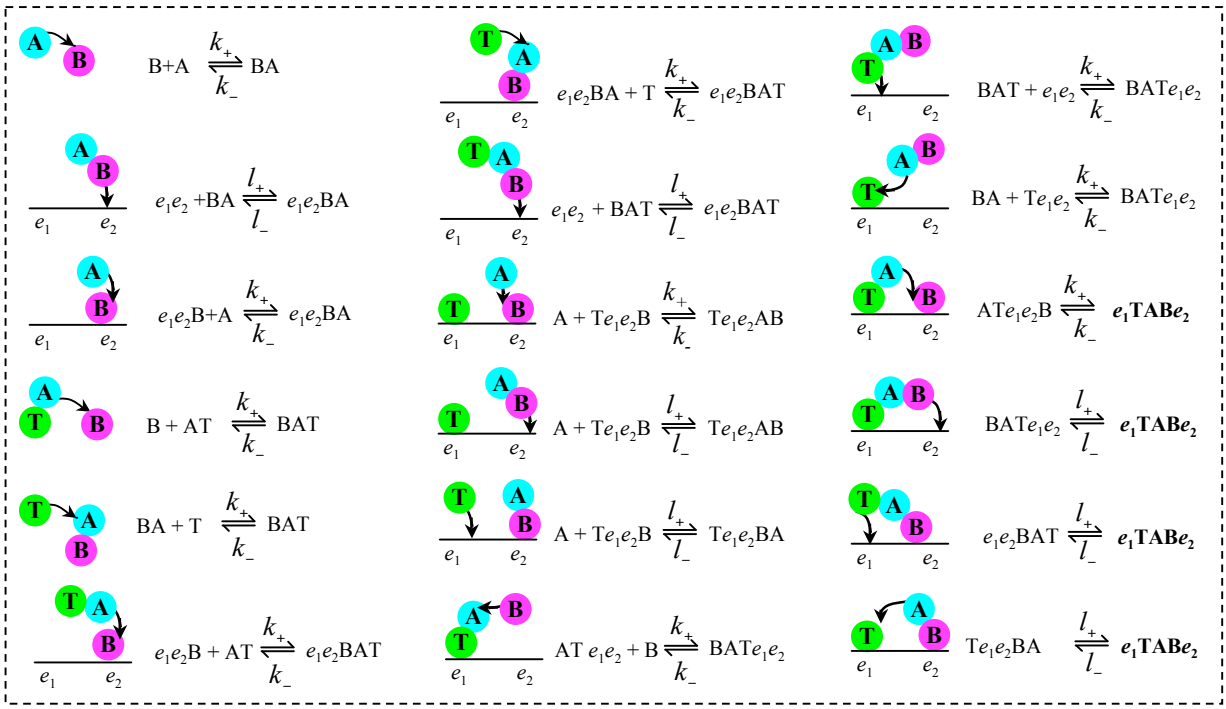

D. Model 2contd: Reactions leading to non-productive complexes in the bridging model (A-B binding)

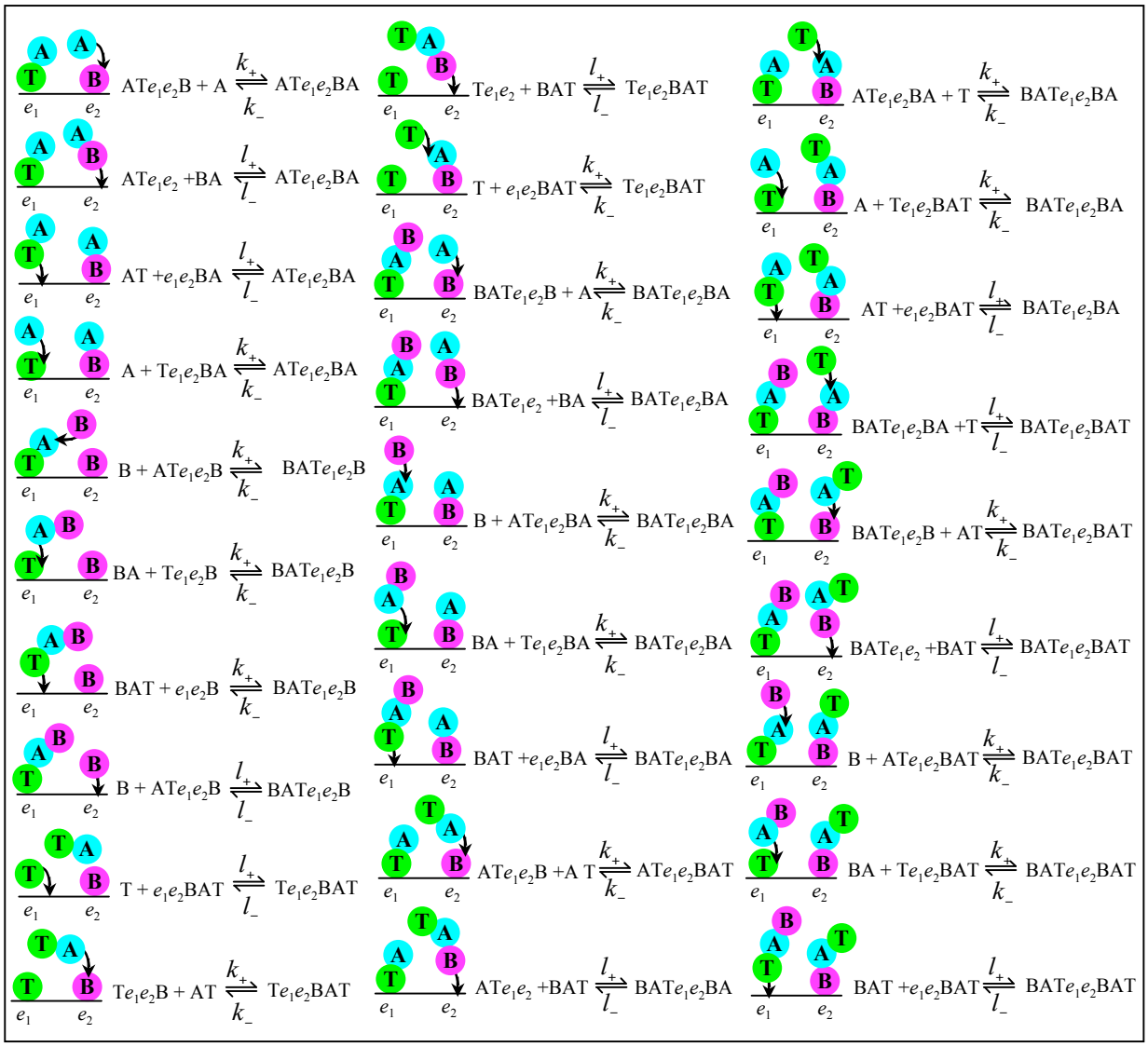

Equations for activation and repression models 1&2 described in Fig S1.

(1) $$\frac{d[A]}{dt} = -k_+[A][Te_3] + k_-[ATe_3] - k_+[A][T] + k_-[AT] - k_+[A][Te_1e_2] + k_-[ATe_1e_2] - k_+[A][Te_1e_2B] + k_-[ATe_1e_2B] + V_A - K_{\deg A}[A] +$$
$$\boxed{-k_+[B][A] + k_-[BA] - k_+[Te_1e_2B][A] + k_-[Te_1e_2BA] - k_+[e_1e_2B][A] + k_-[e_1e_2BA]} +$$
$$\boxed{\begin{aligned} &-k_+[A][Te_1e_2BA] + k_-[ATe_1e_2BA] - k_+[ATe_1e_2B][A] + k_-[ATe_1e_2BA] \\ &-k_+[BATe_1e_2B][A] + e_1e_2k_-[BATe_1e_2BA] - k_+[A][Te_1e_2BAT] + k_-[ATe_1e_2BAT] \end{aligned}}$$

(2) $$\frac{d[B]}{dt} = -l_+[ATe_1e_2][B] + l_-[ATe_1e_2B] - l_+[e_1e_2][B] + l_-[e_1e_2B] - l_+[Te_1e_2][B] + l_-[Te_1e_2B] + V_B - K_{\deg B}[B] +$$
$$\boxed{-k_+[B][A] + k_-[BA] - k_+[B][AT] + k_-[BAT] - k_+[B][ATe_1e_2] + k_-[BATe_1e_2]} +$$
$$\boxed{\begin{aligned} &-l_+[BATe_1e_2][B] + l_-[BATe_1e_2B] - k_+[B][ATe_1e_2BA] + k_-[BATe_1e_2BA] \\ &-k_+[B][ATe_1e_2BAT] + k_-[BATe_1e_2BAT] - k_+[B][ATe_1e_2B] + k_-[BATe_1e_2B] \end{aligned}}$$

(3) $$\frac{d[T]}{dt} = -k_+[A][T] + k_-[AT] - l_+[T][e_1e_2] + l_-[Te_1e_2] - l_+[T][e_3] + l_-[Te_3] - l_+[T][e_1e_2B] + l_-[Te_1e_2B] + V_T - K_{\deg T}[T] +$$
$$\boxed{-k_+[BA][T] + k_-[BAT] - k_+[e_1e_2BA][T] + k_-[e_1e_2BAT] - l_+[T][e_1e_2BA] + l_-[Te_1e_2BA]} +$$
$$\boxed{\begin{aligned} &-l_+[T][e_1e_2BAT] + l_-[Te_1e_2BAT] - k_+[Te_1e_2BA][T] + k_-[Te_1e_2BAT] \\ &-k_+[ATe_1e_2BA][T] + k_-[ATe_1e_2BAT] - k_+[BATe_1e_2BA][T] + k_-[BATe_1e_2BAT] \end{aligned}}$$

(4) $$\boxed{\frac{d[BA]}{dt} = k_+[B][A] - k_-[BA] - k_+[BA][T] + k_-[BAT] - l_+[e_1e_2][BA] + l_-[e_1e_2BA] - k_+[BA][Te_1e_2] + k_-[BAe_1e_2T] - l_+[Te_1e_2][BA] + l_-[Te_1e_2BA]} +$$
$$\boxed{\begin{aligned} &-l_+[ATe_1e_2][BA] + l_-[ATe_1e_2BA] - k_+[BA][Te_1e_2B] + k_-[BATe_1e_2B] - k_+[BA][Te_1e_2BA] + k_-[BATe_1e_2BA] \\ &-l_+[BATe_1e_2][BA] + l_-[BATe_1e_2BA] - k_+[Te_1e_2BAT][BA] + k_-[BATe_1e_2BAT] \end{aligned}}$$

(5) $$\frac{d[AT]}{dt} = l_+[A][T] - l_-[AT] - k_+[B][AT] + k_-[BAT] - l_+[AT][e_1e_2] + l_-[ATe_1e_2] - l_+[AT][e_3] + l_-[ATe_3] - l_+[AT][e_1e_2B] + l_-[ATe_1e_2B] +$$
$$\boxed{-k_+[e_1e_2B][AT] + k_-[e_1e_2BAT]} + \boxed{-l_+[AT][e_1e_2BA] + l_-[ATe_1e_2BA] - k_+[BATe_1e_2B][AT] + k_-[BATe_1e_2BAT]} +$$
$$\boxed{-k_+[Te_1e_2B][AT] + k_-[Te_1e_2BAT] - l_+[AT][e_1e_2BAT] + l_-[ATe_1e_2BAT] - k_+[ATe_1e_2B][AT] + k_-[ATe_1e_2BAT]}$$

(6) $$\frac{d[Te_1e_2]}{dt} = l_+[T][e_1e_2] + l_-[Te_1e_2] - k_+A[Te_1e_2] + k_-[ATe_1e_2] - l_+[Te_1e_2][B] + l_-[Te_1e_2B] +$$
$$\boxed{-k_+[BA][Te_1e_2] + k_-[BATe_1e_2] - l_+[Te_1e_2][BA] + l_-[Te_1e_2BA]} + \boxed{-l_+[Te_1e_2][BAT] + l_-[Te_1e_2BAT]}$$

(7) $$\frac{d[e_1e_2B]}{dt} = l_+[e_1e_2][B] - l_-[e_1e_2B] - l_+[T][e_1e_2B] + l_-[Te_1e_2B] - l_+[AT][e_1e_2B] + l_-[ATe_1e_2B] +$$
$$\boxed{-k_+[e_1e_2B][AT] + k_-[e_1e_2BAT]} + \boxed{-l_+[BAT][e_1e_2B] + l_-[BATe_1e_2B] - k_+[e_1e_2B][A] + k_-[e_1e_2BA]}$$

(8) $$\frac{d[Te_3]}{dt} = l_+[T][e_3] + l_-[Te_3] - k_+A[Te_3] + k_-[ATe_3]$$

(9) $$\frac{d[ATe_3]}{dt} = k_+[A][Te_3] - k_-[ATe_3] + l_+[AT][e_3] - l_-[ATe_3]$$

(10) $$\frac{d[ATe_1e_2]}{dt} = k_+[A][Te_1e_2] - k_-[ATe_1e_2] + l_+[AT][e_1e_2] - l_-[ATe_1e_2] - l_+[ATe_1e_2][B] + l_-[ATe_1e_2B] +$$
$$\boxed{-k_+[B][ATe_1e_2] + k_-[BATe_1e_2]} + \boxed{-l_+[ATe_1e_2][BA] + l_-[ATe_1e_2BA] - l_+[ATe_1e_2][BAT] + l_-[ATe_1e_2BAT]}$$

(11) $$\frac{d[Te_1e_2B]}{dt} = l_+[Te_1e_2][B] - l_-[Te_1e_2B] + l_+[T][e_1e_2B] - l_-[Te_1e_2B] - k_+[A][Te_1e_2B] + k_-[ATe_1e_2B] +$$
$$\boxed{-k_+[Te_1e_2B][A] + k_-[Te_1e_2BA]} + \boxed{-k_+[BA][Te_1e_2B] + k_-[BATe_1e_2B] - k_+[Te_1e_2B][AT] + k_-[Te_1e_2BAT]}$$

(12) $$\boxed{\frac{d[BAT]}{dt} = k_+[B][AT] - k_-[BAT] + l_+[BA][T] - l_-[BAT] - l_+[BAT][e_1e_2] + l_-[BATe_1e_2] - l_+[e_1e_2][BAT] + l_-[e_1e_2BAT]} +$$
$$\boxed{-l_+[Te_1e_2][BAT] + l_-[Te_1e_2BAT] - l_+[BAT][e_1e_2B] + l_-[BATe_1e_2B] - l_+[BAT][e_1e_2BA] + l_-[BATe_1e_2BA]}$$
$$\boxed{-l_+[ATe_1e_2][BAT] + l_-[ATe_1e_2BAT] - l_+[BAT][e_1e_2BAT] + l_-[BATe_1e_2BAT] - l_+[BATe_1e_2][BAT] + l_-[BATe_1e_2BAT]}$$

(13) $$\boxed{\frac{d[e_1e_2BA]}{dt} = l_+[e_1e_2][BA] - l_-[e_1e_2BA] + k_+[e_1e_2B][A] - k_-[e_1e_2BA] - k_+[e_1e_2BA][T] + k_-[e_1e_2BAT] - l_+[T][e_1e_2BA] + l_-[Te_1e_2BA] +}$$
$$\boxed{-l_+[AT][e_1e_2BA] + l_-[ATe_1e_2BA] - l_+[BAT][e_1e_2BA] + l_-[BATe_1e_2BA]}$$

(14) $$\boxed{\frac{d[BATe_1e_2]}{dt} = k_+[B][ATe_1e_2] - k_-[BATe_1e_2] + l_+[BAT][e_1e_2] - l_-[BATe_1e_2] + k_+[BA][Te_1e_2] - k_-[BATe_1e_2]}$$
$$\boxed{- f_1 \cdot l_+[BATe_1e_2] + f_2 \cdot l_-[e_1TABe_2] +}$$
$$\boxed{-l_+[BATe_1e_2][B] + l_-[BATe_1e_2B] - l_+[BATe_1e_2][BA] + l_-[BATe_1e_2BA]}$$

(15) $$\boxed{\frac{d[e_1e_2BAT]}{dt} = l_+[e_1e_2][BAT] - l_-[e_1e_2BAT] + k_+[e_1e_2B][AT] - k_-[e_1e_2BAT] + k_+[e_1e_2BA][T] - k_-[e_1e_2BAT]}$$
$$\boxed{- f_1 \cdot l_+[e_1e_2BAT] + f_2 \cdot l_-[e_1TABe_2] +}$$
$$\boxed{-l_+[T][e_1e_2BAT] + l_-[Te_1e_2BAT] - l_+[AT][e_1e_2BAT] + l_-[ATe_1e_2BAT]}$$

(16) $$\boxed{\frac{d[Te_1e_2BA]}{dt} = l_+[Te_1e_2][BA] - l_-[Te_1e_2BA] + l_+[T][e_1e_2BA] - l_-[Te_1e_2BA] + k_+[Te_1e_2B][A] - k_-[Te_1e_2BA]}$$
$$\boxed{- f_1 \cdot k_+[Te_1e_2BA] + f_2 \cdot k_-[e_1TABe_2] +}$$
$$\boxed{-k_+[A][Te_1e_2BA] + k_-[ATe_1e_2BA] - k_+[Te_1e_2BA][T] + k_-[Te_1e_2BAT] - k_+[BA][Te_1e_2BA] + k_-[BATe_1e_2BA]}$$

(17) $$\frac{d[ATe_1e_2B]}{dt} = l_+[AT][e_1e_2B] - l_-[ATe_1e_2B] + k_+[A][Te_1e_2B] - k_-[ATe_1e_2B] + l_+[ATe_1e_2][B] - l_-[ATe_1e_2B]$$
$$- f_1 \cdot k_+[ATe_1e_2B] + f_2 \cdot k_-[e_1TABe_2] +$$
$$\boxed{-k_+[ATe_1e_2B][A] + k_-[ATe_1e_2BA] - k_+[B][ATe_1e_2B] + k_-[BATe_1e_2B] - k_+[ATe_1e_2B][AT] + k_-[ATe_1e_2BAT]}$$

(18) $$\boxed{\frac{d[e_1TABe_2]}{dt} = f_1 \cdot k_+[ATe_1e_2B] - f_2 \cdot k_-[e_1TABe_2] + f_1 \cdot k_+[Te_1e_2BA] - f_2 \cdot k_-[e_1TABe_2] + f_1 \cdot l_+[e_1e_2BAT] + f_2 \cdot l_-[e_1TABe_2]}$$
$$+ f_1 \cdot l_+[BATe_1e_2] - f_2 \cdot l_-[e_1TABe_2]$$

(19) $$\frac{d[ATe_1e_2BA]}{dt} = k_+[A][Te_1e_2BA] - k_-[ATe_1e_2BA] + l_+[AT][e_1e_2BA] - l_-[ATe_1e_2BA] + k_+[ATe_1e_2B][A] - k_-[ATe_1e_2BA] + l_+[ATe_1e_2][BA] - l_-[ATe_1e_2BA] - k_+[B][ATe_1e_2BA] + k_-[BATe_1e_2BA] - k_+[ATe_1e_2BA][T] + k_-[ATe_1e_2BAT]$$

(20) $$\frac{d[BATe_1e_2B]}{dt} = k_+[B][ATe_1e_2B] - k_-[BATe_1e_2B] + k_+[BA][Te_1e_2B] - k_-[BATe_1e_2B] + l_+[BAT][e_1e_2B] - l_-[BATe_1e_2B] + l_+[BATe_1e_2][B] - l_-[BATe_1e_2B] - k_+[BATe_1e_2B][A] + k_-[BATe_1e_2BA]$$

(21) $$\frac{d[Te_1e_2BAT]}{dt} = l_+[T][e_1e_2BAT] - l_-[Te_1e_2BAT] + k_+[Te_1e_2BA][T] - k_-[Te_1e_2BAT] + k_+[Te_1e_2B][AT] - k_-[Te_1e_2BAT] + l_+[Te_1e_2][BAT] - l_-[Te_1e_2BAT] - k_+[A][Te_1e_2BAT] + k_-[ATe_1e_2BAT]$$

(22) $$\frac{d[BATe_1e_2BA]}{dt} = k_+[B][ATe_1e_2BA] - k_-[BATe_1e_2BA] + k_+[BA][Te_1e_2BA] - k_-[BATe_1e_2BA] + l_+[BAT][e_1e_2BA] - l[BATe_1e_2BA] + l_+[BATe_1e_2][BA] - l_-[BATe_1e_2BA] + k_+[BATe_1e_2B][A] - k_-[BATe_1e_2BA] - k_+[BATe_1e_2BA][T] + k_-[BATe_1e_2BAT]$$

(23) $$\frac{d[ATe_1e_2BAT]}{dt} = l_+[AT][e_1e_2BAT] - l_-[ATe_1e_2BAT] + k_+[A][Te_1e_2BAT] - k_-[ATe_1e_2BAT] + k_+[ATe_1e_2B][AT] - k_-[ATe_1e_2BAT] + l_+[ATe_1e_2][BAT] - l_-[ATe_1e_2BAT] + k_+[ATe_1e_2BA][T] - k_-[ATe_1e_2BAT] - k_+[B][ATe_1e_2BAT] + k_-[BATe_1e_2BAT]$$

(24) $$\frac{d[BATe_1e_2BAT]}{dt} = l_+[BAT][e_1e_2BAT] - l_-[BATe_1e_2BAT] + l_+[BAT][e_1e_2BAT] - l_-[BATe_1e_2BAT] + k_+[BATe_1e_2B][AT] - k_-[BATe_1e_2BAT] + k_+[BA][Te_1e_2BAT] - k_-[BATe_1e_2BAT] + k_+[B][ATe_1e_2BAT] - k_-[BATe_1e_2BAT] + k_+[BATe_1e_2BA][T] - k_-[BATe_1e_2BAT]$$

Descriptions of reactions involved in repression model 3 (direct T•B binding) described in Fig S1.

A. *wg* activation reactions (same as Fig S1)

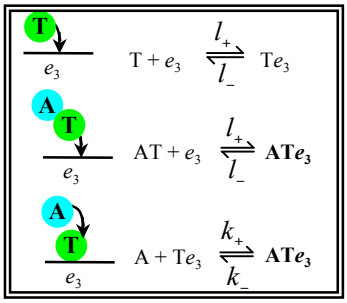

B. Intermediate reactions (same as Model 1, Concurrent binding reactions, Fig S1).

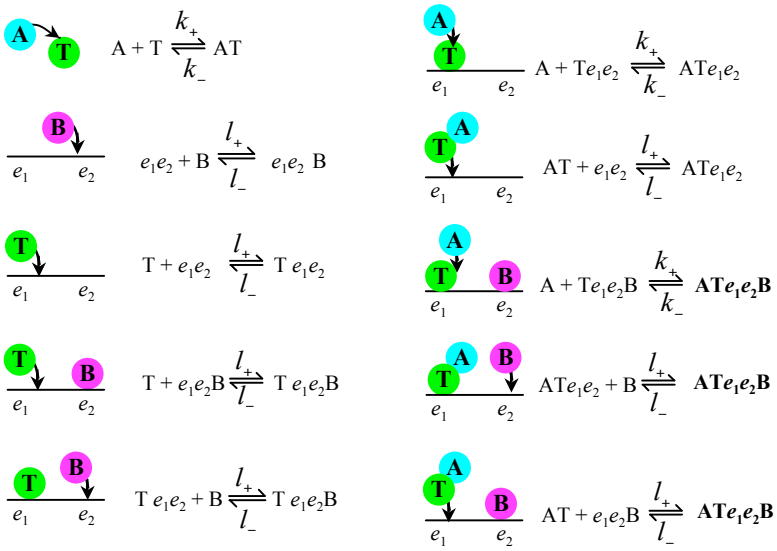

C. Model 3: Reactions leading to productive complexes in the direct T•B binding model

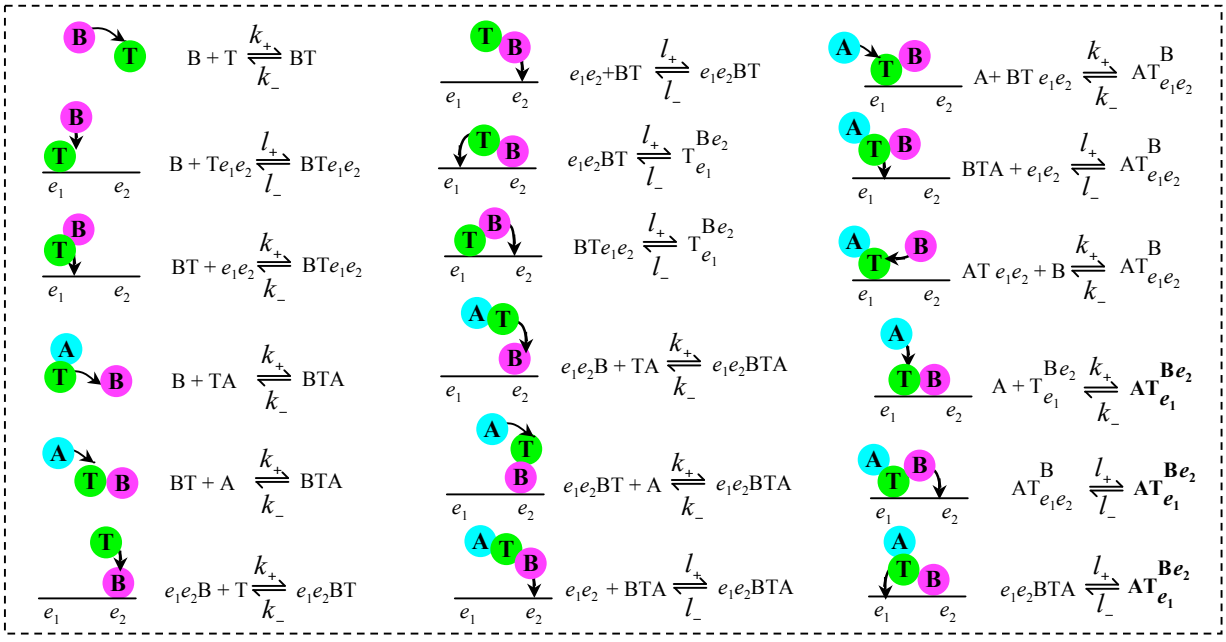

D. Model 3contd: Reactions leading to non-productive complexes in the direct T•B binding model

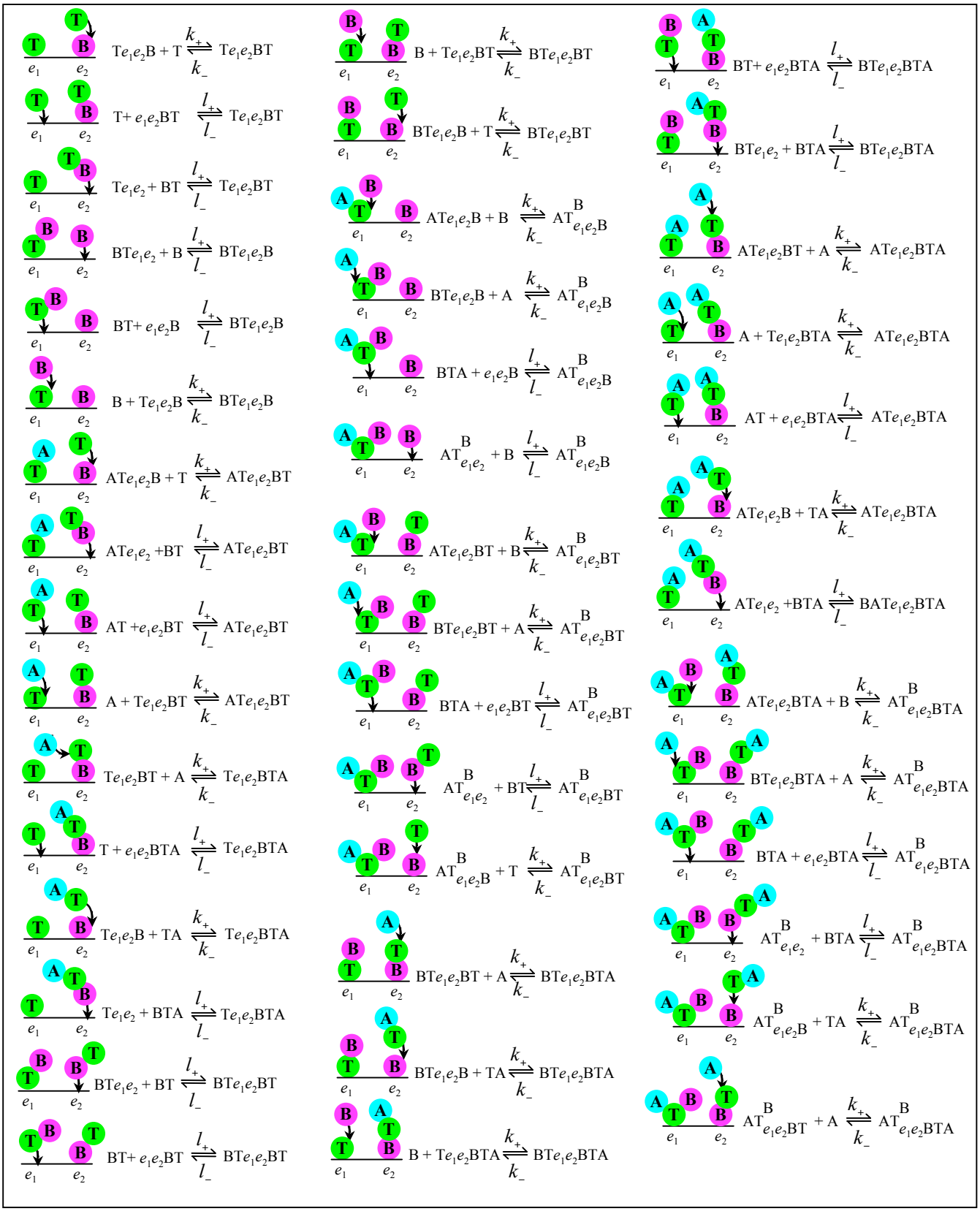

Equations for repression model 3 (direct T•B binding) described in Fig S1.

(1') $$\frac{d[A]}{dt} = -k_+[A][Te_3] + k_-[ATe_3] - k_+[A][T] + k_-[AT] - k_+[A][Te_1e_2] + k_-[ATe_1e_2] - k_+[A][Te_1e_2B] + k_-[ATe_1e_2B] + V_A - K_{\deg A}[A] +$$
$$-k_+[BT][A] + k_-[BTA] - k_+[A][BTR] + k_-[AT^B_{e_1e_2}] - k_+[RBT][A] + k_-[RBTA] - k_+[A][T^{Be_2}_{e_1}] + k_-[AT^{Be_2}_{e_1}] +$$
$$-k_+[A][Te_1e_2BT] + k_-[ATe_1e_2BT] - k_+[Te_1e_2BT][A] + k_-[Te_1e_2BTA] - k_+[BTe_1e_2BT][A] + k_-[BTe_1e_2BTA]$$
$$-k_+[ATe_1e_2BT][A] + k_-[ATe_1e_2BTA] - k_+[AT^B_{e_1e_2BT}][A] + k_-[AT^B_{e_1e_2BTA}] - k_+[A][BTe_1e_2B] + k_-[AT^B_{e_1e_2B}]$$
$$-k_+[BTe_1e_2BT][A] + k_-[AT^B_{e_1e_2BT}] - k_+[A][Te_1e_2BTA] + k_-[ATe_1e_2BTA]$$

(2') $$\frac{d[B]}{dt} = -l_+[ATe_1e_2][B] + l_-[ATe_1e_2B] - l_+[e_1e_2][B] + l_-[e_1e_2B] - l_+[Te_1e_2][B] + l_-[Te_1e_2B] + V_B - K_{\deg B}[B] +$$
$$-k_+[B][T] + k_-[BT] - k_+[B][TA] + k_-[BTA] - k_+[B][Te_1e_2] + k_-[BTe_1e_2] - k_+[ATe_1e_2][B] + k_-[AT^B_{e_1e_2}] +$$
$$-k_+[B][Te_1e_2B] + k_-[BTe_1e_2B] - l_+[BTe_1e_2][B] + l_-[BTe_1e_2B] - k_+[B][Te_1e_2BT] + k_-[BTe_1e_2BT] - k_+[B][Te_1e_2BTA] + k_-[BTe_1e_2BTA]$$
$$-k_+[ATe_1e_2BTA][B] + k_-[AT^B_{e_1e_2BTA}] - l_+[AT^B_{e_1e_2}][B] + l_-[AT^B_{e_1e_2B}] - k_+[ATe_1e_2B][B] + k_-[AT^B_{e_1e_2B}] - k_+[ATe_1e_2BT][B] + k_-[AT^B_{e_1e_2BT}]$$

(3') $$\frac{d[T]}{dt} = -k_+[A][T] + k_-[AT] - l_+[T][e_1e_2] + l_-[Te_1e_2] - l_+[T][e_3] + l_-[Te_3] - l_+[T][e_1e_2B] + l_-[Te_1e_2B] + V_T - K_{\deg T}[T] +$$
$$-k_+[B][T] + k_-[BT] - k_+[e_1e_2B][T] + k_-[e_1e_2BT] +$$
$$-l_+[T][e_1e_2BT] + l_-[Te_1e_2BT] - k_+[Te_1e_2B][T] + k_-[Te_1e_2BT] - l_+[ATe_1e_2B][T] + l_-[ATe_1e_2BT]$$
$$-k_+[BTe_1e_2B][T] + k_-[BTe_1e_2BT] - l_+[T][e_1e_2BTA] + l_-[Te_1e_2BTA] - k_+[AT^B_{e_1e_2B}][T] + k_-[AT^B_{e_1e_2BT}]$$

(4') $$\frac{d[BT]}{dt} = k_+[B][T] - k_-[BT] - k_+[BT][A] + k_-[BTA] - l_+[BT][e_1e_2] + l_-[BTe_1e_2] - l_+[e_1e_2][BT] + l_-[e_1e_2BT] +$$
$$-l_+[Te_1e_2][BT] + l_-[Te_1e_2BT] - l_+[BT][e_1e_2B] + l_-[BTe_1e_2B] - l_+[ATe_1e_2][BT] + l_-[ATe_1e_2BT] - l_+[BT][e_1e_2BT] + l_-[BTe_1e_2BT]$$
$$-l_+[BTe_1e_2][BT] + l_-[BTe_1e_2BT] - l_+[BT][e_1e_2BTA] + l_-[BTe_1e_2BTA] - l_+[AT^B_{e_1e_2}][BT] + l_-[AT^B_{e_1e_2BT}]$$

(5') $$\frac{d[AT]}{dt} = k_+[A][T] - k_-[AT] - l_+[AT][e_1e_2] + l_-[ATe_1e_2] - l_+[AT][e_3] + l_-[ATe_3] - l_+[AT][e_1e_2B] + l_-[ATe_1e_2B] +$$
$$-k_+[B][AT] + k_-[BTA] - k_+[e_1e_2B][AT] + k_-[e_1e_2BTA] +$$
$$-l_+[AT][e_1e_2BT] + l_-[ATe_1e_2BT] - k_+[Te_1e_2B][AT] + k_-[Te_1e_2BTA] - k_+[BTe_1e_2B][AT] + k_-[BTe_1e_2BTA]$$
$$-l_+[AT][e_1e_2BTA] + l_-[ATe_1e_2BTA] - k_+[ATe_1e_2B][AT] + k_-[ATe_1e_2BTA] - k_+[AT^B_{e_1e_2B}][AT] + k_-[AT^B_{e_1e_2BTA}]$$

(6') $$\frac{d[Te_1e_2]}{dt} = l_+[T][e_1e_2] + l_-[Te_1e_2] - k_+A[Te_1e_2] + k_-[ATe_1e_2] - l_+[Te_1e_2][B] + l_-[Te_1e_2B] +$$
$$-k_+[B][Te_1e_2] + k_-[BTe_1e_2] + -l_+[Te_1e_2][BT] + l_-[Te_1e_2BT] - l_+[Te_1e_2][BTA] + l_-[Te_1e_2BTA]$$

(7') $$\frac{d[e_1e_2B]}{dt} = l_+[e_1e_2][B] - l_-[e_1e_2B] - l_+[T][e_1e_2B] + l_-[Te_1e_2B] - l_+[AT][e_1e_2B] + l_-[ATe_1e_2B] +$$
$$-k_+[e_1e_2B][T] + k_-[e_1e_2BT] - k_+[e_1e_2B][TA] + k_-[e_1e_2BTA] + -l_+[BT][e_1e_2B] + l_-[BTe_1e_2B] - l_+[BTA][e_1e_2B] + l_-[AT^B_{e_1e_2B}]$$

(8') $$\frac{d[Te_3]}{dt} = l_+[T][e_3] + l_-[Te_3] - k_+A[Te_3] + k_-[ATe_3]$$

(9') $$\frac{d[ATe_3]}{dt} = k_+[A][Te_3] - k_-[ATe_3] + l_+[AT][e_3] - l_-[ATe_3]$$

(10') $$\frac{d[ATe_1e_2]}{dt} = k_+[A][Te_1e_2] - k_-[ATe_1e_2] + l_+[AT][e_1e_2] - l_-[ATe_1e_2] - l_+[ATe_1e_2][B] + l_-[ATe_1e_2B] +$$
$$\boxed{-k_+[ATe_1e_2][B] + k_-[AT^B_{e_1e_2}]} + \boxed{-l_+[ATe_1e_2][BT] + l_-[ATe_1e_2BT] - l_+[ATe_1e_2][BTA] + l_-[ATe_1e_2BTA]}$$

(11') $$\frac{d[Te_1e_2B]}{dt} = l_+[Te_1e_2][B] - l_-[Te_1e_2B] + l_+[T][e_1e_2B] - l_-[Te_1e_2B] - k_+[A][Te_1e_2B] + k_-[ATe_1e_2B] +$$
$$\boxed{-k_+[Te_1e_2B][A] + k_-[Te_1e_2BA]} + \boxed{-k_+[Te_1e_2B][T] + k_-[Te_1e_2BT] - k_+[B][Te_1e_2B] + k_-[BTe_1e_2B] - k_+[Te_1e_2B][AT + k_-[Te_1e_2BTA]}$$

(12') $$\boxed{\frac{d[BTA]}{dt} = k_+[B][TA] - k_-[BTA] + l_+[BT][A] - l_-[BTA] - l_+[BTA][e_1e_2] + l_-[AT^B_{e_1e_2}]}$$
$$\boxed{-l_+[e_1e_2][BTA] + l_-[e_1e_2BTA] - l_+[e_1e_2][BTA] + l_-[AT^{Be_2}_{e_1}] +}$$
$$\boxed{\begin{aligned}&-l_+[Te_1e_2][BTA] + l_-[Te_1e_2BTA] - l_+[ATe_1e_2][BTA] + l_-[ATe_1e_2BTA] - l_+[BTA][e_1e_2B] + l_-[AT^B_{e_1e_2B}] - l_+[BTA][e_1e_2BT]\\&+ l_-[AT^B_{e_1e_2BT}] - l_+[AT^B_{e_1e_2}][BTA] + l_-[AT^B_{e_1e_2BTA}] - l_+[BTA][e_1e_2BTA] + l_-[AT^B_{e_1e_2BTA}] - l_+[BTe_1e_2][BTA] + l_-[BTe_1e_2BTA]\end{aligned}}$$

(13') $$\boxed{\frac{d[e_1e_2BT]}{dt} = l_+[e_1e_2][BT] - l_-[e_1e_2BT] + k_+[e_1e_2B][T] - k_-[e_1e_2BT] - l_+[e_1e_2BT] + l_-[T^{Be_2}_{e_1}] - l_+[e_1e_2BT][A] + l_-[e_1e_2BTA]} +$$
$$\boxed{-l_+[T][e_1e_2BT] + l_-[Te_1e_2BT] - l_+[AT][e_1e_2BT] + l_-[ATe_1e_2BT] - l_+[BT][e_1e_2BT] + l_-[BTe_1e_2BT] - l_+[BTA][e_1e_2BT] + l_-[AT^B_{e_1e_2BT}]}$$

(14') $$\boxed{\frac{d[BTe_1e_2]}{dt} = l_+[BT][e_1e_2] - l_-[BTe_1e_2] + k_+[B][Te_1e_2] - k_-[BTe_1e_2] - l_+[BTe_1e_2] + l_-[T^{Be_2}_{e_1}] - k_+[A][BTe_1e_2] + k_-[AT^B_{e_1e_2}]} +$$
$$\boxed{-l_+[BTe_1e_2][B] + l_-[BTe_1e_2B] - l_+[BTe_1e_2][BT] + l_-[BTe_1e_2BT] - l_+[BTe_1e_2][BTA] + l_-[BTe_1e_2BTA]}$$

(15') $$\boxed{\frac{d[T^{Be_2}_{e_1}]}{dt} = l_+[BTe_1e_2] - l_-[T^{Be_2}_{e_1}] + l_+[e_1e_2BT] - l_-[T^{Be_2}_{e_1}] - k_+[A][T^{Be_2}_{e_1}] + k_-[AT^{Be_2}_{e_1}]}$$

(16') $$\boxed{\frac{d[AT^B_{e_1e_2}]}{dt} = k_+[ATe_1e_2][B] - k_-[AT^B_{e_1e_2}] + l_+[BTA][e_1e_2] - l_-[AT^B_{e_1e_2}] + k_+[A][BTe_1e_2] - k_-[AT^B_{e_1e_2}]}$$
$$\boxed{-l_+[AT^B_{e_1e_2}][B] + l_-[AT^B_{e_1e_2B}] - l_+[AT^B_{e_1e_2}][BT] + l_-[AT^B_{e_1e_2BT}] - l_+[AT^B_{e_1e_2}][BTA] + l_-[AT^B_{e_1e_2BTA}]}$$
$$\boxed{-l_+[AT^B_{e_1e_2}][BT] + l_-[AT^B_{e_1e_2BT}] - l_+[AT^B_{e_1e_2}][BTA] + l_-[AT^B_{e_1e_2BTA}]}$$

(17') $$\boxed{\frac{d[e_1e_2BTA]}{dt} = l_+[e_1e_2][BTA] - l_-[e_1e_2BTA] + k_+[e_1e_2B][AT] - k_-[e_1e_2BTA] + k_+[e_1e_2BT][A] - k_-[e_1e_2BTA]}$$
$$\boxed{-f_1 \cdot l_+[e_1e_2BTA] + f_2 \cdot l_-[AT^{Be_2}_{e_1}] +}$$
$$\boxed{\begin{aligned}&-l_+[T][e_1e_2BTA] + l_-[Te_1e_2BTA] - l_+[BT][e_1e_2BTA] + l_-[BTe_1e_2BTA] - l_+[AT][e_1e_2BTA] + l_-[ATe_1e_2BTA]\\&-l_+[BTA][e_1e_2BTA] + l_-[AT^B_{e_1e_2BTA}]\end{aligned}}$$

(18') $$\frac{d[ATe_1e_2B]}{dt} = l_+[AT][e_1e_2B] - l_-[ATe_1e_2B] + k_+[A][Te_1e_2B] - k_-[ATe_1e_2B] + l_+[ATe_1e_2][B] - l_-[ATe_1e_2B]$$
$$\boxed{-k_+[ATe_1e_2B][A] + k_-[ATe_1e_2BA] - k_+[ATe_1e_2B][AT] + k_-[ATe_1e_2BTA] - k_+[ATe_1e_2B][B] + k_-[AT^B_{e_1e_2B}]}$$

(19') $$\boxed{\frac{d[AT^{Be_2}_{e_1}]}{dt} = k_+[A][T^{Be_2}_{e_1}] - k_-[AT^{Be_2}_{e_1}] + k_+[e_1e_2][BTA] - k_-[AT^{Be_2}_{e_1}] + f_1 \cdot l_+[e_1e_2BTA] + f_2 \cdot l_-[AT^{Be_2}_{e_1}]}$$

(20') $$\frac{d[Te_1e_2BT]}{dt} = l_+[T][e_1e_2BT] - l_-[Te_1e_2BT] + l_+[Te_1e_2][BT] - l_-[Te_1e_2BT] + k_+[Te_1e_2B][T] - k_-[Te_1e_2BT] - k_+[A][Te_1e_2BT] + k_-[ATe_1e_2BT] - l_+[B][Te_1e_2BT] + l_-[BTe_1e_2BT] - k_+[Te_1e_2BT][A] + k_-[Te_1e_2BTA]$$

(21') $$\frac{d[BTe_1e_2B]}{dt} = k_+[B][Te_1e_2B] - k_-[BTe_1e_2B] + l_+[BT][e_1e_2B] - l_-[BTe_1e_2B] - k_+[BTe_1e_2B][T] + k_-[BTe_1e_2BT] + l_+[BTe_1e_2][B] - l_-[BTe_1e_2B] - k_+[BTe_1e_2B][AT] + k_-[Te_1e_2BTA] - k_+[A][BTe_1e_2B] + k_-[AT^B_{e_1e_2B}]$$

(22') $$\frac{d[ATe_1e_2BT]}{dt} = k_+[A][Te_1e_2BT] - k_-[ATe_1e_2BT] + l_+[AT][e_1e_2BT] - l_-[ATe_1e_2BT] + k_+[ATe_1e_2B][T] - k_-[ATe_1e_2BT] + l_+[ATe_1e_2][BT] - l_-[ATe_1e_2BT] - k_+[ATe_1e_2BT][A] + k_-[ATe_1e_2BTA] - k_+[ATe_1e_2BT][B] + k_-[AT^B_{e_1e_2BT}]$$

(23') $$\frac{d[BTe_1e_2BT]}{dt} = k_+[B][Te_1e_2BT] - k_-[BTe_1e_2BT] + l_+[BT][e_1e_2BT] - l_-[BTe_1e_2BT] + k_+[BTe_1e_2B][T] - k_-[BTe_1e_2BT] + l_+[BTe_1e_2][BT] - l_-[BTe_1e_2BT] - k_+[BTe_1e_2BT][A] + k_-[Te_1e_2BTA] - k_+[A][BTe_1e_2BT] + k_-[AT^B_{e_1e_2BT}]$$

(24') $$\frac{d[Te_1e_2BTA]}{dt} = k_+[Te_1e_2BT][A] - k_-[Te_1e_2BTA] + l_+[T][e_1e_2BTA] - l_-[Te_1e_2BTA] + k_+[Te_1e_2B][AT] - k_-[Te_1e_2BTA] + l_+[Te_1e_2][BTA] - l_-[Te_1e_2BTA] - k_+[B][Te_1e_2BTA] + k_-[BTe_1e_2BTA] - k_+[A][Te_1e_2BTA] + k_-[ATe_1e_2BTA]$$

(25') $$\frac{d[BTe_1e_2BTA]}{dt} = k_+[B][Te_1e_2BTA] - k_-[BTe_1e_2BTA] + l_+[BT][e_1e_2BTA] - l_-[BTe_1e_2BTA] + l_+[BTe_1e_2][BTA] - l_-[BTe_1e_2BTA] + k_+[BTe_1e_2BT][A] - k_-[BTe_1e_2BTA] + k_+[BTe_1e_2B][AT] - k_-[BTe_1e_2BTA] - k_+[A][BTe_1e_2BTA] + k_-[AT^B_{e_1e_2BTA}]$$

(26') $$\frac{d[ATe_1e_2BTA]}{dt} = k_+[A][Te_1e_2BTA] - k_-[ATe_1e_2BTA] + l_+[AT][e_1e_2BTA] - l_-[ATe_1e_2BTA] + l_+[ATe_1e_2][BTA] - l_-[ATe_1e_2BTA] + k_+[ATe_1e_2B][AT] - k_-[ATe_1e_2BTA] - k_+[ATe_1e_2BTA][B] + k_-[AT^B_{e_1e_2BTA}]$$

(27') $$\frac{d[AT^B_{e_1e_2B}]}{dt} = k_+[A][BTe_1e_2B] - k_-[AT^B_{e_1e_2B}] + l_+[BTA][e_1e_2B] - l_-[AT^B_{e_1e_2B}] + l_+[AT^B_{e_1e_2}][B] - l_-[AT^B_{e_1e_2B}] + k_+[ATe_1e_2B][B] - k_-[AT^B_{e_1e_2B}] - k_+[AT^B_{e_1e_2B}][T] + k_-[AT^B_{e_1e_2BT}] - k_+[AT^B_{e_1e_2B}][AT] + k_-[AT^B_{e_1e_2BTA}]$$

(28') $$\frac{d[AT^B_{e_1e_2BT}]}{dt} = k_+[A][BTe_1e_2BT] - k_-[AT^B_{e_1e_2BT}] + l_+[BTA][e_1e_2BT] - l_-[AT^B_{e_1e_2BT}] + l_+[AT^B_{e_1e_2B}][T] - l_-[AT^B_{e_1e_2BT}] + k_+[ATe_1e_2BT][B] - k_-[AT^B_{e_1e_2BT}] + l_+[AT^B_{e_1e_2}][BT] - l_-[AT^B_{e_1e_2BT}] - k_+[AT^B_{e_1e_2BT}][A] + k_-[AT^B_{e_1e_2BTA}]$$

(29') $$\frac{d[AT^B_{e_1e_2BTA}]}{dt} = k_+[A][BTe_1e_2BTA] - k_-[AT^B_{e_1e_2BTA}] + l_+[BTA][e_1e_2BTA] - l_-[AT^B_{e_1e_2BTA}] + k_+[AT^B_{e_1e_2B}][AT] - k_-[AT^B_{e_1e_2BTA}] + k_+[ATe_1e_2BTA][B] - k_-[AT^B_{e_1e_2BTA}] + l_+[AT^B_{e_1e_2}][BTA] - l_-[AT^B_{e_1e_2BTA}] + k_+[AT^B_{e_1e_2BT}][A] - k_-[AT^B_{e_1e_2BTA}]$$

Fig. S6
Theisen et. al